

How to build a magnetometer with thermal atomic vapor: A tutorial

Anne Fabricant^{1,2}, Irina Novikova³, and Georg Bison⁴

¹Helmholtz Institute Mainz, GSI Helmholtzzentrum für Schwerionenforschung, Darmstadt, Germany

²Johannes Gutenberg University of Mainz, Mainz, Germany

³Department of Physics, William & Mary, Williamsburg, Virginia 23187, USA

⁴Paul Scherrer Institute, Villigen 5232, Switzerland

Abstract. This article is designed as a step-by-step guide to optically pumped magnetometers based on alkali atomic vapor cells. We begin with a general introduction to atomic magneto-optical response, as well as expected magnetometer performance merits and how they are affected by main sources of noise. This is followed by a brief comparison of different magnetometer realizations and an overview of current research, with the aim of helping readers to identify the most suitable magnetometer type for specific applications. Next, we discuss some practical considerations for experimental implementations, using the case of an M_z magnetometer as an example of the design process. Finally, an interactive workbook with real magnetometer data is provided to illustrate magnetometer-performance analysis.

1. Why should you build an atomic magnetometer?

The purpose of this review is to introduce students and newcomers to the field of atomic magnetometry in a friendly and didactic manner. We aim to bridge the gap between the various excellent reviews already existing in literature [1–7] and the nitty-gritty of actually setting up and operating an atomic magnetometer in the lab, for either academic or industrial purposes.

The origins of magnetometry — the measurement of magnetic fields — most likely date back to the time of the dinosaurs 150 million years ago, when the first birds evolved. It is known that birds, not only those of the migratory variety, possess an innate magnetic compass for orientation along the geomagnetic field lines, which is activated by exposure to light [8, 9]. In fact, a wide range of animal species are blessed with built-in geomagnetic-field sensors, based on a variety of proposed biochemical mechanisms [10]. Humans, being less gifted by nature, had to develop their own navigational compasses — the earliest type of magnetometer — through arduous scientific work from the 12th century onward, enabling the formation of empires in Europe and Asia. After Gauss developed, in 1832, the first known absolute magnetometer able to directly measure the geomagnetic field, the 20th century saw an explosion of new magnetometer technologies

based on both classical- and quantum-physics phenomena. This enabled the sensitive measurement of hypogeomagnetic fields (fields smaller than Earth field) from a diversity of sources (Table 1). Chances are that the reader is routinely carrying around a state-of-the-art magnetometer: most modern smartphones are outfitted with a tiny Hall-effect or magnetoresistive (MR) based compass, which can be integrated onto a chip with an accelerometer (to sense linear acceleration) and usually a gyroscope (to sense angular acceleration).

Atomic magnetometers are quantum devices making use of the fact that the electron spin of each atom in a gas reacts to its own magnetic-field environment. During magnetometer operation, atoms are first spin-polarized via optical pumping with laser light along a given direction (Sec. 2.1), then allowed to evolve under the influence of an external magnetic field (Sec. 2.3). Magnetic-field measurement is enabled by subsequent optical readout of the atomic spin state, which exploits magneto-optical effects — for example, shining linearly polarized off-resonant “probe” light on the atoms and measuring its polarization rotation via the Faraday effect, or measuring the change in absorption of resonant probe light (Sec. 2.5). Such atomic magnetometers may be called by different names, including optical(-atomic) magnetometers or optically pumped magnetometers (OPMs), although the magnetic-sensing volume itself consists of atoms.

Before designing and building a sensor in the lab, one should first ask an important question: *Is atomic magnetometry right for my application?* There exists a plethora of magnetometer technologies, many of which are commercially available, with each technology having its own pros and cons. In Table 1 and Fig. 1, we compare the performance figures of some common commercial magnetometers operating in the magnetic-field range up to Earth field.

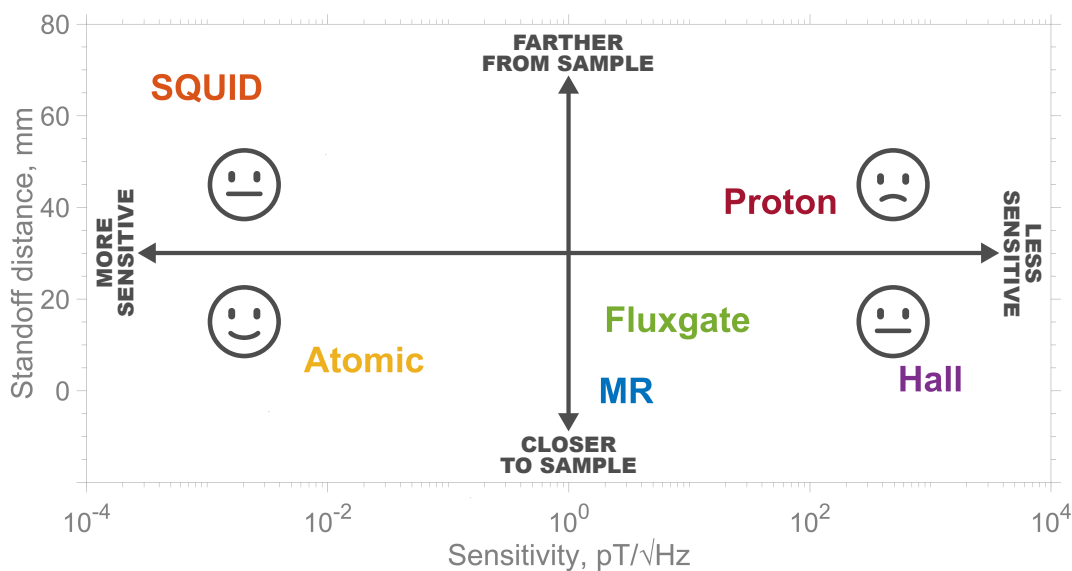


Figure 1: A silly pictorial representation of the information in Table 1.

Fig. 1 illustrates that atomic magnetometers can offer the best overall performance for applications requiring both relatively high magnetic-field sensitivity and relatively

Sensor type	Birth year	Example(s)	Sensitivity (pT/ $\sqrt{\text{Hz}}$)	Standoff distance (mm)	Smallest linear dimension (mm)	Bandwidth (kHz)	Approx. price range (USD)	Notes
Fluxgate	1936 [11]	SENSYS, Bartington	6–10	14.5–16.5	23–26	3–4	3–5 000	better lab sensitivity achieved [12, 13]
Proton (incl. Overhauser)	1958 [14]	GEM, Geometrics	15–100	37.5–45	75–90	15–30	100–1 000	geophysical applications
Atomic	1962 [15]	QuSpin, Twinleaf	0.01–0.03 (0.09–0.13)	6.5	12.4	0.10–0.15 (0.5–1.1)	9–10 000	biomedical applications
SQUID	1964 [16]	Quantum Design, Magnicon	0.001	66	840	1	up to 1 000 000	cheaper partial systems available
Hall-effect	1967 [17]	Metrolab	1000	2.5	1.2	1	4–10 000	useful for field mapping
Magnetoresistive	1982 [18]	TE Connectivity, Sensitec	3	0	N/A	10	2 000	only bare sensor sold commercially

Table 1: Performance comparison of commonly available commercial magnetometers. The choice of examples is intended to be representative and not exhaustive; quoted specs are approximate. Non-commercial laboratory magnetometers may surpass the quoted typical performance figures [19]. See Sec. 3 for definitions and discussion of the performance figures. Note that optically pumped magnetometers based on nitrogen-vacancy (NV) centers in diamond [20] are not included in this table, since commercial NV sensors at the time of writing are sold only as scanning-microscopy imaging systems. Atomic magnetometers based on parametric resonance in He-4 are currently undergoing commercialization by the company MAG4Health.

small stand-off distance from the sample to be measured. Unlike superconducting-quantum-interference-device (SQUID) magnetometers, they are non-cryogenic and can operate at ambient temperatures, while also offering greater portability. Although the leading commercial models are designed specifically for biomedical applications such as magnetoencephalography (MEG) [21] and fetal magnetocardiography (fMCG) [22], there is great flexibility in the design of laboratory atomic magnetometers. For example, the atomic sensing volume can be miniaturized or otherwise adapted to the particular sample geometry [23, 24].

This review is structured as follows. In Sec. 2, we briefly introduce the technique of optical pumping, through which atomic-spin polarization can be created using resonant laser light. Then we present what we consider to be the most important equation of magnetometry, the Bloch equation, which describes the interaction of atomic spins with an external magnetic field — the heart of an atomic magnetometer. To illustrate the process of magnetometer operation, we consider a specific example of an M_z magnetometer. Sec. 3 provides an overview of the relevant figures of merit used to characterize magnetometer performance, some of which were already introduced in Table 1. Sec. 4 compares the different types of atomic magnetometers and guides the reader in selecting an appropriate operating mode for the desired application (e.g.,

biological/non-biological, applied/fundamental) and performance requirements. From Sec. 5, the tutorial becomes more hands-on. Here we describe how to choose proper components for the magnetometer, including a suitable atomic vapor cell for the sensing volume, as well as laser and magnetic-shielding systems. Next, we outline the step-by-step operational principles of the M_z magnetometer and describe how to obtain a free-induction-decay (FID) signal — steps which can be applied by the reader to other types of atomic magnetometers. Sec. 6 focuses on how to characterize magnetometer performance according to the figures of merit discussed in Sec. 3.

As the title of this review suggests, we will be covering magnetometers based on thermal atomic vapors. In cold-atom magnetometry, laser cooling is employed to trap and control the sensing atoms, and to prevent spin-destructive atomic collisions which worsen magnetometer performance (Sec. 3). Although cold atoms offer advantages in terms of spatial resolution and stand-off distance, the experimental requirements are more stringent and require the use of a vacuum system, and the number of atoms which can be trapped is limited. Despite progress in recent years [25, 26], the sensitivity of cold-atom sensors is not yet competitive with thermal sensors utilizing buffer-gas or anti-relaxation-coated atomic vapor cells (Sec. 5.1). Therefore, the latter are preferred for most atomic-magnetometry applications (Sec. 7).

Furthermore, we focus specifically on alkali-vapor sensing. References are provided for readers interested in learning more about magnetic sensing with nuclear or electron spins in helium [27–33], as well as comagnetometers incorporating both noble-gas and alkali vapors in tandem, whereby the nuclear-spin signal is enhanced via spin-exchange optical pumping [34, 35]. Helium magnetometers have traditionally been used for military and aerospace applications, due to their intrinsic robustness and stability, and optically pumped He-4 sensors have recently begun to approach the sensitivity levels of their alkali cousins [28, 36]. Alkali/noble-gas comagnetometers are primarily used in fundamental-physics and gyroscope experiments [34, 37–40].

2. The Bloch equation and all that jazz

This section introduces the methodology for theoretical modeling of an atomic magnetometer. As a starting point for the concrete description of such a magnetometer, we choose the experimental setup shown in Fig. 2A. The core of the magnetometer is the alkali atoms which form a vapor in a glass cell. A laser beam traverses the cell, and the power of the transmitted light is measured by a photodiode. Since atoms interact with both the ambient magnetic field \vec{B} and the laser light, they mediate magneto-optical coupling, such that information about \vec{B} is transferred to the measurable optical signal. At the level of individual atoms, this interaction is characterized by the total atomic angular momentum \vec{F} , often referred to as the atomic spin. However, since the laser beam interacts with a large number of atoms at the same time, the ensemble average of \vec{F} is the relevant quantity here. This ensemble average, which we denote as \vec{M} , is a macroscopic quantity describing the magnetization state of the atomic medium.

Because \vec{M} is derived from atomic spins, it is a macroscopic sum of atomic angular momenta. In the atomic-magnetometry literature, \vec{M} is commonly referred to as the **bulk magnetization** or just **magnetization** of the atomic medium. (We note that in electromagnetism, \vec{M} is defined as bulk magnetization per unit volume.)

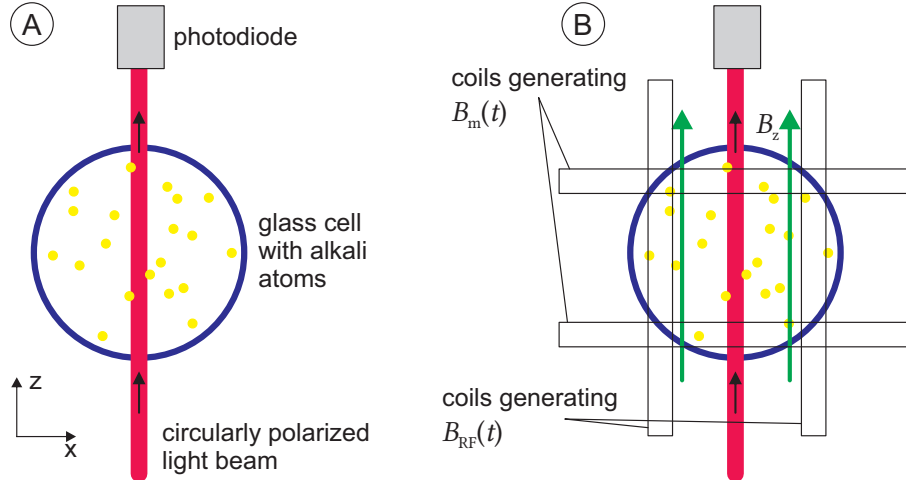


Figure 2: A) Basic setup of an optically pumped magnetometer. B) Setup for the M_z mode of operation.

Although in this section we primarily rely on the classical description of spin dynamics, we'll first briefly introduce some basics of the quantum description which are relevant for understanding. Our chosen theoretical treatment of the magnetometer can be described as semiclassical, where quantum mechanics is only explicitly invoked in the discussion of optical pumping (Sec. 2.1). We find that this approach, based on classical Bloch formalism, is typically the most intuitive and accessible for new experimentalists. However, we wish to emphasize that physically equivalent quantum treatments are also possible. These include the density-matrix formalism — whereby the atomic spin state is encoded in multipole moments of a density matrix which evolves, e.g. in the presence of any electromagnetic fields, according to the quantum Liouville equation [41, 42] — as well as the Floquet description [43] and representations within the framework of quantum optics [44].

In spectroscopic notation, the electronic energy levels of an atom are denoted nL_J . Here n is the principal quantum number and \vec{L} is the orbital angular momentum with quantum number L ($S=0$, $P=1$, $D=2$); $\vec{J} = \vec{L} + \vec{S}$ is the total electronic angular momentum, with \vec{S} being the electron spin ($S = 1/2$). The total angular momentum of the atom is then $\vec{F} = \vec{I} + \vec{J}$, where \vec{I} is the nuclear spin. Let us take as an example the alkali atom Cs-133, the only stable isotope of cesium, with $I = 7/2$: the ground state $6S_{1/2}$ ($\vec{L} = 0$) splits into two hyperfine states with $F = 3$ and $F = 4$.

Atomic magnetometers make use of this **hyperfine structure** of electronic energy levels, which arises from the magnetic interaction between the nucleus and the electron. The magnetic structure becomes experimentally discernible as a result of the **Zeeman effect**, whereby the otherwise-degenerate hyperfine energy levels split in the presence

of a static magnetic field (linearly, in the low-field regime). Summing over all N atomic spins in the ensemble gives us the bulk magnetization:

$$\vec{M} = \sum_{n=1}^N \vec{F}_n. \quad (1)$$

Both quantities, \vec{F}_n and \vec{M} , can be measured experimentally from outside the medium [45, 46].

The magnetic quantum number $m_F = F, F - 1, \dots, -F$ measures the atomic-spin component along a given quantization axis. In the absence of optical pumping with laser light (Sec. 2.1), each atom's m_F -substates will be thermally populated — corresponding to an unpolarized medium in which the atomic spins are randomly oriented, with an average magnetization given by $\vec{M} = 0$. This is the state which the medium always tends to approach, due to various effects that disturb the atomic spins and thus randomize them. If we are able to put most of the atoms into one of the extreme hyperfine substates $m_F = \pm F$, we have achieved macroscopic spin polarization along the direction of the quantization axis — which manifests classically as bulk magnetization — and we say that there is **orientation** of the atomic-spin ensemble. The spin state of an individual fully polarized atom, in $m_F = \pm F$, is known as a “stretched state”.

Other interesting situations are possible: some magnetometers utilize atomic-spin **alignment** — similar to orientation in the sense that there is a preferred polarization *axis*, but different in that there is no preferred polarization *direction*. Alignment is important for atomic magnetometers based on the principle of nonlinear magneto-optical rotation (NMOR), described in Sec. 4. The concept of orientation-to-alignment conversion is treated in a didactic and visual way in [47].

Note that throughout this tutorial and in other atomic-physics literature, the word “polarization” is commonly used to refer to both atomic-spin polarization and light polarization (direction of the light electric field). We hope that the distinction will be clear from the context, such that this overlapping terminology does not cause confusion.

2.1. Optical pumping

The first step toward making the medium useful for magnetometry purposes is to create spin polarization, equivalent to magnetizing the medium: orienting a sizeable fraction of the atomic spins in the same direction. In nuclear-magnetic-resonance (NMR) experiments this is typically achieved using a strong (few T) magnet, but alkali atoms can be much more efficiently magnetized using optical pumping. Optical pumping is a field of atomic physics in itself, and a detailed treatment may be found in the canonical reference [48]. For our purposes it suffices to say that using the Hamiltonian for a light-atom dipole interaction, one can derive the following angular-momentum **selection**

rules for the driven atomic transitions:

$$\Delta L = \pm 1, \quad (2)$$

$$\Delta S = 0, \quad (3)$$

$$\Delta J = \pm 1, 0, \quad (4)$$

$$\Delta F = \pm 1, 0. \quad (5)$$

We see that a photon can transfer angular momentum, but it does not interact with the electron spin. The selection rules for the magnetic quantum numbers depend on the polarization of the light. For circularly polarized light, we have

$$\sigma_+ \text{ photon} \Rightarrow \Delta m_F = +1, \quad (6)$$

$$\sigma_- \text{ photon} \Rightarrow \Delta m_F = -1. \quad (7)$$

Here σ_+ and σ_- denote, respectively, right- and left-circular polarization. When we talk about circular polarization, we should be clear about the convention we are using for handedness. If we visualize the light as a classical wave, σ_+ (σ_-) polarization means that the polarization vector is rotating in the clockwise (counterclockwise) direction *as seen from the source*. An atom may also decay by spontaneous emission with $\Delta m_F = \pm 1, 0$. Examples of the pumping process in alkali atoms are illustrated in Appendix A and in [49, 50].

Thus, the first interaction we need in our model is the absorption of circularly polarized photons by the atoms, in order to create orientation in the atomic ground state. Each photon carries a quantum of angular momentum which is transferred to the atoms. As a consequence, \vec{M} builds up in the direction of the laser beam. This build-up can be modeled classically by the following differential equation:

$$\frac{d}{dt} \begin{pmatrix} M_x(t) \\ M_y(t) \\ M_z(t) \end{pmatrix} = \Gamma_p \begin{pmatrix} 0 - M_x(t) \\ 0 - M_y(t) \\ M_p - M_z(t) \end{pmatrix} - \Gamma_r \begin{pmatrix} M_x(t) \\ M_y(t) \\ M_z(t) \end{pmatrix}. \quad (8)$$

Here, Γ_p is the pumping rate, Γ_r is the relaxation rate due to as-yet-unspecified relaxation mechanisms (for now assumed to be the same for all magnetization components), and M_p is the maximum magnetization which can be achieved in the absence of relaxation according to this equation, such that eventually $M_p/M_z = 1$. This expression explicitly assumes that the laser-light direction is parallel to the z -axis, as shown in Fig. 2. The pumping rate quantifies how fast the optical pumping works and is proportional to the power of the laser beam. We see that in the absence of relaxation mechanisms, any magnetization in the x - or y -directions tends toward 0 with a rate Γ_p , while the magnetization in the z -direction approaches the value M_p .

Eq. (8) can be simplified by defining an effective relaxation rate $\Gamma = \Gamma_p + \Gamma_r$ and an effective asymptotic (steady-state) magnetization $M_a = M_p \Gamma_p / \Gamma$, which yields

$$\frac{d}{dt} \begin{pmatrix} M_x(t) \\ M_y(t) \\ M_z(t) \end{pmatrix} = \Gamma \begin{pmatrix} -M_x(t) \\ -M_y(t) \\ M_a - M_z(t) \end{pmatrix}. \quad (9)$$

This means that in the general case of optical pumping along the z -direction, any magnetization in the x - or y -directions tends toward 0 with a rate Γ , while the magnetization in the z -direction approaches the value M_a .

Traditionally, the electromagnetic field that creates the magnetization is referred to as **pump** light, and the one that is used to detect it as **probe** light. However, in many magnetometer arrangements, light from the same laser plays both roles. If all atomic spins in the medium are parallel or antiparallel to the direction of the laser beam — i.e., each atom is in a stretched state, having the maximum amount of angular momentum with respect to the light direction — no atom can absorb a photon, since it would be physically impossible to transfer even more angular momentum to the atom. Thus, the medium has become transparent to the laser light. In general, one can detect the direction of atomic magnetization optically, since the amount of light transmitted through the medium is proportional to the projection of \vec{M} onto the light wavenumber \vec{k} . In most systems, transmission is high (absorption is low) for \vec{M} parallel to \vec{k} , while transmission is low (absorption is high) for \vec{M} antiparallel to \vec{k} . Further discussion of optical detection is provided in Sec. 2.5.

Figure 3 shows how the magnetization accumulates after optical pumping is started at time $t = 0$. Time is measured in units of the characteristic relaxation time $T_1 \equiv 1/\Gamma_r$, and amplitude is measured in units of M_p . The different curves show how the magnetization behavior changes as a function of laser power, proportional to the pumping rate Γ_p . All quantities in the graph are dimensionless, and thus the curves are universally applicable when the scaling coefficients Γ_p and M_p are known. Since the transmitted light power is proportional to $\vec{M}(t)$, the displayed curves can be easily measured.

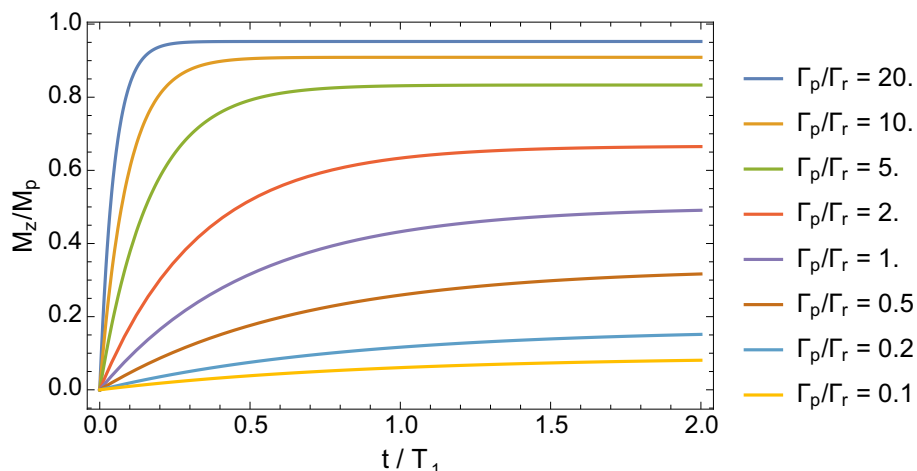


Figure 3: Simulation of atomic magnetization as it can be measured by monitoring transmitted light power as a function of time. The different curves show the magnetization behavior for different laser powers and thus different pumping rates Γ_p , defined with respect to the spin relaxation rate Γ_r . For $\Gamma_p/\Gamma_r = 20$, a spin-ensemble polarization of approximately 95% is achieved.

Solving Eq. (9) yields

$$M_z(t) = M_a (1 - e^{-\Gamma t}) = M_p \frac{\Gamma_p}{\Gamma_r + \Gamma_p} [1 - e^{-(\Gamma_r + \Gamma_p)t}] . \quad (10)$$

With increasing laser power, the asymptotic magnetization M_a comes closer to its maximum value, given by M_p . It is also evident that the time constant of the exponential approach to steady state is shortened by increasing the laser power. Solving for the steady state, we find that optical pumping alone gives

$$\frac{d}{dt} \begin{pmatrix} M_x(t) \\ M_y(t) \\ M_z(t) \end{pmatrix} = 0 \quad \Rightarrow \quad \begin{pmatrix} M_x(t) \\ M_y(t) \\ M_z(t) \end{pmatrix} = \begin{pmatrix} 0 \\ 0 \\ M_a \end{pmatrix} . \quad (11)$$

2.2. Spin-relaxation times

Let us assume that we are able to create a high degree of magnetization $M_z/M_p \approx 1$ along the z -direction via optical pumping. Looking at Eq. (8), we see that if we then turn off the pump beam at time $t = 0$ such that $\Gamma_p = 0$, the longitudinal magnetization decays as

$$M_z(t) = M_z(0) e^{-\Gamma_r t} = M_p e^{-t/T_1} , \quad (12)$$

Here we have explicitly introduced the traditional **spin-depopulation time** $T_1 = 1/\Gamma_r$, which describes how fast the atomic magnetization decays to the unpolarized thermal state — or, in the presence of a longitudinal magnetic field, to a nonzero equilibrium magnetization.

What happens to the magnetization components transverse to the pumping direction, M_x and M_y , in this case? Until now, we have assumed that the transverse and longitudinal relaxation rates are the same. Although it is possible to add by hand different relaxation rates for each magnetization component in Eq. (8), here we begin to reach the limits of the classical description. According to our modeling thus far, in the absence of any additional electromagnetic fields (Sec. 2.3), after optical pumping we should effectively have $M_x = 0 = M_y$. This is not the full picture, however, since atomic magnetometers are quantum devices which make use of **spin coherence**. Although the expectation value of each atomic spin along either transverse direction is zero, there are nonzero quantum fluctuations in accordance with the Heisenberg uncertainty principle, as discussed further in Sec. 3.1. In the density-matrix description of the atomic spin state [41, 42], the diagonal elements of the density matrix give the m_F -sublevel population probabilities, while the off-diagonal elements represent the coherences (superpositions) among sublevels. These coherences give rise to the transverse spin components, which also decay exponentially with a time constant called the **spin-(de)coherence time** T_2 . As explained in Sec. 3.1, the T_2 time is a crucial parameter which defines the sensitivity of an atomic magnetometer. In general, the longer the T_1 time in an atomic ensemble, the longer will be the T_2 time as well. Although typically $T_1 \geq T_2$, for purposes of calculation it is often convenient to set $T_1 \approx T_2$. In thermal atomic vapor cells, a dominant spin-relaxation mechanism is collision of atoms with the cell walls (Sec. 5.1).

2.3. Interaction of atoms with a magnetic field

Apart from optical pumping, the second interaction that drives an atomic magnetometer is the effect of external magnetic fields on the magnetization \vec{M} of the medium. A magnetic field acting on polarized atoms induces a torque that aims to align the magnetization with the field lines. Since the magnetization results from atomic spins with angular momentum, this torque induces a precession motion of the spins, known as Larmor precession. The precession frequency or **Larmor frequency** Ω is proportional to the magnetic field, and it is convenient to express all magnetic-field components in terms of precession frequencies. For example, we define for the x -component $\Omega_x = \gamma B_x$, with the gyromagnetic ratio γ (see [51] for the γ values of different alkali atoms). This allows us to model the evolution of M in the following way:

$$\frac{d}{dt} \begin{pmatrix} M_x(t) \\ M_y(t) \\ M_z(t) \end{pmatrix} = \begin{pmatrix} M_x(t) \\ M_y(t) \\ M_z(t) \end{pmatrix} \times \begin{pmatrix} \Omega_x \\ \Omega_y \\ \Omega_z \end{pmatrix} + \Gamma \begin{pmatrix} -M_x(t) \\ -M_y(t) \\ M_a - M_z(t) \end{pmatrix}. \quad (13)$$

The first part of this expression is the classical Bloch equation, which has been extended to model optical pumping along the z -direction as well as relaxation of the magnetization. The equation is useful for a basic description of virtually all processes in optically pumped atomic magnetometers. For example, it defines how the optical absorptive and dispersive properties of the atomic medium are modified, which enables optical detection of the change in spin state as discussed in Sec. 2.5.

More detailed descriptions of the atom-field interaction can be derived from quantum density-matrix calculations [41, 42, 52].

2.4. A specific example: Measuring the transverse magnetic field

Let us have a look at some special cases. First, we assume that we have a magnetic field parallel to the laser beam. In this situation, the pumping process creates magnetization only along the magnetic-field direction. The field induces precession around an axis given by the field direction, which in this case does not change the magnetization at all. Due to the cross-product in Eq. (13), the z -component of the field mixes the x - and y -components of the magnetization, which are zero in this case. Thus, the situation is stable, and we find the same result as in Eq. (11).

The situation changes when we apply a magnetic field along a direction perpendicular to z — for example, the x -direction. When we solve for the steady state (by setting the time derivatives equal to zero) with $\Omega_y = 0$ and $\Omega_z = 0$, Eq. (13) simplifies to

$$\frac{d}{dt} \begin{pmatrix} M_x(t) \\ M_y(t) \\ M_z(t) \end{pmatrix} = \begin{pmatrix} -\Gamma M_x \\ M_z \Omega_x - \Gamma M_y \\ -M_y \Omega_x + \Gamma (M_a - M_z) \end{pmatrix} = \begin{pmatrix} 0 \\ 0 \\ 0 \end{pmatrix}. \quad (14)$$

Apart from the trivial result $M_x = 0$, this equation contains the essence of many atomic magnetometers. In the term for M_y , two contributions have to balance each other in the steady state. The first contribution is a source term that increases the modulus of M_y proportionally to Ω_x , by rotating magnetization from the z -direction to the y -direction. The second contribution is the relaxation, which decreases the modulus of M_y .

The term for M_z has similar contributions, which here have reversed roles. The first one models the loss of M_z as it is rotated to M_y , and the second one is a relaxation towards the asymptotic magnetization M_a . Solving the system of equations yields

$$M_y = M_a \frac{\Gamma \Omega_x}{\Gamma^2 + \Omega_x^2} = M_a \frac{x}{1 + x^2}, \quad M_z = M_a \frac{\Gamma^2}{\Gamma^2 + \Omega_x^2} = M_a \frac{1}{1 + x^2}, \quad (15)$$

where $x = \Omega_x/\Gamma$ is a dimensionless variable that expresses the magnetic-field component scaled to the corresponding precession frequency and divided by the relaxation rate. Both M_y and M_z show resonant behavior, and the dimensionless parameterization allows us to generate the universally applicable plots shown in Fig. 4.

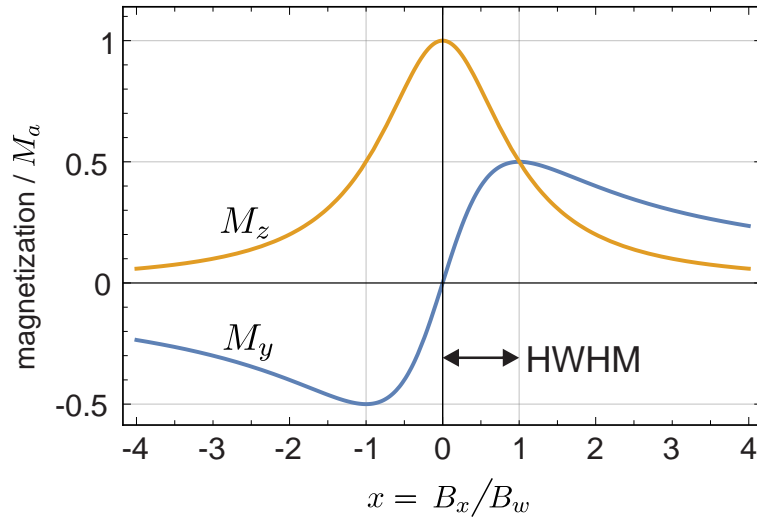


Figure 4: Magnetic-resonance spectrum for the case $B_y = B_z = 0$. The M_y and M_z components of the magnetization show resonant behavior as a function of B_x . The scale for the x -axis is given by the magnetic linewidth B_w . M_y displays a dispersive and M_z an absorptive Lorentzian resonance.

The amplitude of both resonances is given by the asymptotic magnetization M_a . When $B_x = 0$ and consequently $x = 0$, M_z reaches M_a and M_y vanishes. This is the same situation as in Eq. (11) for optical pumping alone. The magnetization M_z shows an absorptive Lorentzian peak and thus gets smaller with an increasing magnitude of B_x . At $x = \pm 1$, we find $M_z = M_a/2$; this means that the half width at half maximum (HWHM) gives the points where the modulus of the precession frequency Ω_x is equal to the relaxation rate Γ . We can define the magnetic linewidth B_w by rearranging the terms that define x :

$$x = \frac{\gamma B_x}{\Gamma} = \frac{B_x}{B_w}, \quad \text{with} \quad B_w = \frac{\Gamma}{\gamma}.$$

This concept is not limited to the x -component of B , as we shall see in Sec. 5.4.

The M_y component follows a dispersive Lorentzian curve with a linear zero crossing. Close to $x = 0$, the M_y component is thus proportional to the applied magnetic field. The larger the change in magnetization signal (relative to noise) produced by a small change in the magnetic field, the more sensitive the magnetometer. This exact method is used in magnetometers based on the ground-state Hanle effect, also known as zero-field resonance, which often operate in the spin-exchange-relaxation-free (SERF) regime (see Sec. 4).

2.5. Optical detection

The propagation of light through an atomic medium can be modeled semiclassically, whereby the electronic energy levels are quantized but the light is treated as a classical electromagnetic field in which the electrons are oscillating dipoles [53]. Based on its electric polarizability, the atomic medium has a complex index of refraction for light:

$$n(\omega) = n_{\text{Re}}(\omega) + i n_{\text{Im}}(\omega) , \quad (16)$$

expressed as a function of the angular frequency ω of the incident light. Here n_{Re} defines the real index of refraction, characterized by dispersive behavior as a function of ω ; n_{Im} defines the absorption, characterized by resonant behavior at the resonance frequency $\omega = \omega_0$. At resonance, $n_{\text{Re}} = 0$ and $n_{\text{Im}} = 1$, in analogy to the behavior of the magnetization curves in Fig. 4. This duality enables two different modes of optical detection in atomic magnetometry, either absorptive (based on light transmission) or dispersive (based on light polarization rotation).

An external magnetic field creates birefringence in the atomic medium, such that the σ_+ and σ_- polarization components of incident light along the magnetic-field direction experience different values of n . Depending on the detection mode, this manifests as a change in absorption or polarization rotation of the transmitted probe light. In both cases, the change is proportional to the projection of the atomic magnetization in the direction of light propagation, from which the Larmor frequency can be extracted.

3. Define your requirements: Figures of merit

When designing a magnetometer, the following questions should first be considered in order to select an appropriate operating mode (Sec. 4). They relate the application requirements to associated magnetometer performance figures, some of which were already introduced in Sec. 1.

- (i) What are the amplitude and frequency ranges of the signals I want to measure? → **sensitivity, bandwidth**
- (ii) How close must the sensing volume be to the sample? How well do I need to localize the measured signals? → **standoff distance, spatial resolution**
- (iii) Am I interested in measuring absolute or relative field values? → **accuracy**

(iv) Over what time scale do I plan to measure? → **stability**

3.1. Sensitivity and noise

Sensitivity to magnetic fields is arguably the most important benchmark used to characterize magnetometer performance. In atomic magnetometry, sensitivity is typically reported in units of T/ $\sqrt{\text{Hz}}$ (SI) or G/ $\sqrt{\text{Hz}}$ (CGS). Although these units may appear mysterious to newcomers, they can be understood by noting that magnetic-field noise fluctuates over the frequency bandwidth of a magnetometer. In order to measure sensitivity, one records the magnetometer response for some time duration. To convert from the time domain to the frequency domain, a fast Fourier transform is performed to produce a magnetic-field-noise power spectrum (see Sec. 6). Calculating root-mean-square (RMS) amplitudes of the noise in 1 Hz bins leads to a sensitivity expressed per $\sqrt{\text{Hz}}$. Note that although both sensitivity and **resolution** are essentially a measure of the smallest change in magnetic field detectable by the sensor (at a given frequency), the units are different — resolution is reported in magnetic-field units alone.

For measurement of relatively small magnetic fields, we would like the sensitivity of our magnetometer to be as good as possible — in the ideal case, limited only by fundamental quantum mechanics. It is important to identify the various contributions to noise in our measurements, and to understand how they behave.

The basic sensitivity limits for an atomic magnetometer are set by the Heisenberg uncertainty principle, which manifests in the **spin-projection noise** δB_{PN} of the atoms and the **shot noise** δB_{SN} of the probe light. These contributions to the magnetometer sensitivity scale as [1]

$$\delta B_{\text{PN}} \propto \frac{1}{\sqrt{N T_2 t}}, \quad (17)$$

$$\delta B_{\text{SN}} \propto \frac{1}{\sqrt{\Phi t}}, \quad (18)$$

where N is the number of atoms in the ensemble, T_2 is the spin-coherence time of the ensemble introduced in Sec. 2.2, Φ is the photon flux of the probe light, and t is the total measurement time. We see that noise decreases the longer we measure, corresponding to a better sensitivity and underscoring the value of averaging over many measurement cycles. In order to express Eqs. (17–18) as noise densities (per $\sqrt{\text{Hz}}$), we can multiply by \sqrt{t} .

Spin-projection noise is a type of **atomic noise** that ultimately limits the sensitivity of any atomic magnetometer regardless of the particular modality or detection method. In order to understand this limit, it is instructive to consider a single atom. Imagine that we prepare the atom in a stretched state along the z -direction, as described in Sec. 2, and then measure the atomic-spin projection m_F along some axis. If this experiment is repeated a number of times, we find the expectation value $\langle F_z \rangle = F$. Along the x - and y -directions we measure zero on average, but each individual measurement yields a

random result according to the uncertainty principle:

$$\Delta F_x \Delta F_y \geq \frac{\langle F_z \rangle}{2}, \quad (19)$$

which in the case of the minimum-uncertainty stretched state becomes

$$\Delta F_x \Delta F_y = \frac{F}{2}. \quad (20)$$

A derivation of Eq. (17) may be found in Appendix B. As explained in quantum-optics textbooks, it is possible to beat the limit set by Eq. (20) for ΔF_x or ΔF_y (but not both simultaneously) via a technique known as **spin squeezing**, such that the magnetometer sensitivity may be improved [54]. Squeezing of the probe light may also be employed to beat sensitivity limits set by photon shot noise. Such “quantum-enhanced” atomic magnetometry is an active area of research [55–61].

Another quantum-mechanical source of atomic noise is **back-action noise**. This stems from the fundamental problem of not being able to measure a quantum system without disturbing it. In the case of atomic magnetometry, we use light as a detection tool since we cannot read out the atomic spin states directly. This interference by the experimenters results in “back action” of the light onto the atoms — essentially an AC Stark shift, also known as light shift, caused by the probe light which shifts the hyperfine energy levels and changes the Larmor precession frequency. In effect, a “fictitious magnetic field” is generated on top of the real one that we actually want to measure. Various evasion techniques have been developed for reducing or eliminating back-action noise [62, 63]. Since, in contrast to shot noise (Eq. (18)), the contribution of back-action noise to sensitivity scales as $\sqrt{\Phi}$, one does not generally gain by increasing probe power — which can also introduce additional atomic noise due to undesirable depumping effects.

In practice, there may be additional systematic sources of noise that worsen the sensitivity of a magnetometer, including **electronic noise** and **technical (classical) noise**. These categories are, of course, somewhat artificial, as some electronic noise may be classical. Furthermore, some classical noise may be atomic — according to our definition, atomic noise is anything that causes **broadening** of the magnetic resonance. Since the resonance linewidth is inversely proportional to the spin-coherence time T_2 , sensitivity worsens in the presence of any such broadening. One common source of classical atomic noise is magnetic-field gradients. Systematics are discussed further in Sec. 4.2.

Whether or not it is necessary to suppress systematic noise sources enough to achieve so-called quantum-noise-limited operation depends on the application requirements. In any case, it is considered best practice to remove electronic noise from the photodetector signal by measuring and subtracting dark counts. For detection modalities based on light polarization rotation (Sec. 4), many classical noise sources can be removed via homodyne-detection schemes, a common technique in quantum optics

[64]. Absorption-based detection modalities, while generally simpler to implement, are more prone to systematics due to, e.g., laser-intensity noise.

Going back to Eq. (17), we also see that in order to optimize sensitivity — i.e., to make it as small as possible — one should increase both the number of atoms and the coherence time inside the vapor cell. The latter can be accomplished in two ways: (1) by using **antirelaxation wall coating** that has low absorption energy for the atoms, so that they spend less time at the cell walls, or (2) by using a **buffer gas** to prevent atoms from diffusing to the walls. Both these techniques, which are discussed further in Sec. 5.1, are effective because spin relaxation at the cell walls is a key relaxation mechanism [65, 66]. A popular way to increase the density of atoms is by heating the vapor cell — SERF magnetometers work at temperatures over 100°C (Sec. 4).

3.2. Bandwidth and spatial performance

One often hears the statement that in magnetometry, there exists a trade-off between sensitivity and bandwidth, i.e. that improving the sensitivity comes at the cost of reduced bandwidth and vice versa. This is because these two parameters tend to have an opposite dependence on the the width of the atomic resonance. Narrow resonances may provide better sensitivity (which is good), but smaller bandwidth (which is usually bad). Another way to think about this intuitively is to recall that bandwidth gives us information about how quickly a magnetometer responds to sudden changes in magnetic field: the smaller the change to which the magnetometer is sensitive, the longer it takes for the magnetometer to react to this change. A directly related concept is **dynamic range**, or the range of field magnitudes that can be measured within the magnetometer response bandwidth.

The sensitivity-bandwidth trade-off is not the only one arising in the context of magnetometer performance figures. We have already seen that we want to maximize the number of atoms in the sensing volume, as per Eq. (17). Naively, this suggests that we should make the sensing volume as large as possible. Regardless of the cell volume, for atoms in thermal motion, the probe light effectively interacts with all atoms equally, such that the motion of individual atoms averages out and we can think of the light as addressing a homogeneous atomic ensemble, a principle known as motional averaging. In the case of buffer-gas cells, where the atoms are prevented from diffusing to the cell walls, the size of the probe beam is typically chosen to interact with a majority of atoms in the cell. However, a larger volume tends to increase the sensor standoff distance and decrease the spatial resolution of measurements.

More precisely, the standoff distance of a sensor is generally defined as the distance between the sample of interest and the geometric center of the sensing volume; the spatial resolution is the smallest spatial variation in the measured signal that can be resolved. Thus, we may run into trouble if we want to localize signals to within distance scales smaller than the diameter of the sensing volume. One way around this is to decrease the size of the sensing volume but increase the atomic density via heating, ideally in the

SERF regime. Arrays of miniaturized vapor cells can be used to obtain excellent spatial localization and mapping of magnetic signals (Secs. 4.2 and 5.1). An alternative way to effectively increase the atomic density, by actually increasing the light-atom interaction, is to place the vapor cell in an optical cavity or to use a multipass cell [67–70].

3.3. Stability and accuracy

Stability essentially refers to how long a magnetometer can operate continuously, or continually in pulsed mode, before it needs to be recalibrated. For example, some popular commercially available sensors operate at zero field via integrated field coils which null the local magnetic field. However, any drifts in the local magnetic-field environment over time eventually push the sensor out of its sensitive range, limiting the duration of continuous magnetometer operation. For longer-term sensor usage demanding greater stability with limited power consumption, e.g. in non-lab settings, a self-oscillating mode of operation is preferred which renders the magnetometer insensitive to such drifts; the NMOR magnetometers discussed in Sec. 4 are ideal in this case. Feedback control of various other time-dependent sensor parameters, such as laser frequency and cell temperature, is typically also required for practical operation. A standard way to quantify the stability of a magnetometer, or other frequency-based measurement device, is to calculate the Allan variance over time [71].

Finally, the accuracy of a sensor has to do with whether we are measuring absolute or relative magnetic-field values — in the latter case, this performance figure is less critical. In essence, magnetometers measure frequencies which must be converted to corresponding magnetic-field values. For some applications, such as precise mapping of the geomagnetic field and other coarse magnetic structures, or precise measurement of physical constants, accuracy is paramount and may outrank sensitivity as the dominant figure of merit [31, 72]. Since atoms form the heart of the magnetometers under consideration here, these can be used as an absolute reference during magnetometer calibration, in order to improve accuracy. In practice, however, various systematics may worsen measurement accuracy during magnetometer operation (Sec. 4.2).

4. Choose your operating mode

As discussed in Sec. 2, most atomic magnetometers have a similar underlying physical principle of operation, relying on a resonant change in either light absorption or rotation of the light polarization to determine the Larmor precession frequency and extract the magnetic-field value. Yet, this operational principle allows for many different configurations, each having its own strengths and weaknesses. The choice of a particular approach is usually dictated by the desired magnetometer performance and other application-specific restrictions. In this section, we provide a brief comparative analysis of the main approaches for magnetic-field measurements and their basic performance characteristics, as summarized in Table 2.

Magnetometer type	Mz	Mx	Bell-Bloom	Hanle/SERF	NMOR	CPT/EIT
Typical geometry						
Operational principle	Circularly polarized light \vec{E}_0 , parallel to the bias magnetic field \vec{B}_0 , magnetizes atoms along the z -axis. An orthogonal resonant RF field at the Larmor frequency produces a narrow absorption resonance [15, 73].	Circularly polarized light \vec{E}_0 propagates at an angle to the bias magnetic field \vec{B}_0 and along the oscillating RF field. Light absorption is defined by the transverse magnetization component [15, 74–76].	Intensity modulation of the laser light \vec{E}_0 produces stroboscopic optical pumping when modulated at the Larmor frequency [77, 78].	Circularly polarized pump light \vec{E} sets the atomic magnetization, whose orientation imprints on the polarization angle of a weak probe \vec{E}_0 . Often operates in the spin-exchange relaxation-free (SERF) regime [67, 79].	Linearly polarized light \vec{E}_0 aligns the atoms, whose precession in the magnetic field \vec{B}_0 imprints on the light polarization angle [80–82]. Use of the modulated light enables operation at nonzero magnetic field [83, 84].	A bichromatic optical field $\vec{E}_{1,2}$ prepares atoms in a superposition of magnetosensitive hyperfine sublevels with increased transmission (“dark state”) [85, 86].
Sensitivity, fT/ $\sqrt{\text{Hz}}$	10 [87]	1 [74]	20 [88–90]	0.16 [91]	70 [92]	10,000 [86, 93]
Bandwidth, kHz	0.6 [87]	1 [94, 95]	1 [90]	1 [95, 96]	> 100 [97]	> 0.1 [98, 99]
Can operate at Earth field?	yes	yes	yes	no	yes	yes
Has been modified for vector measurement?	no	[100]	[69, 101, 102]	[103, 104]	[105, 106]	[107]
Miniaturization: cell volume sensor volume sensitivity	1 mm ³ 22 cm ³ 15 pT/ $\sqrt{\text{Hz}}$ [108, 109]	2 mm ³ 25 mm ³ 5 pT/ $\sqrt{\text{Hz}}$ [108, 110, 111]	16 mm ³ NA 0.07 pT/ $\sqrt{\text{Hz}}$ [111–113]	6 mm ³ NA 0.07 pT/ $\sqrt{\text{Hz}}$ [96, 114]	$7 \cdot 10^{-4}$ mm ³ NA 700 pT/ $\sqrt{\text{Hz}}$ [115]	1 mm ³ 12 mm ³ 50 pT/ $\sqrt{\text{Hz}}$ [116, 117]

Table 2: Brief summary of the main atomic-magnetometer technologies.

4.1. Common types of atomic magnetometers

We saw in Sec. 2.1 that many atomic magnetometers rely on circularly polarized light, tuned near one of the atomic optical transitions, to optically pump atoms and create the desired magnetization of the atomic ensemble. Among these devices, summarized in the first four columns of Table 2, the most common are probably M_z and M_x magnetometers, so named for the magnetization component to which the device is sensitive. Both of them utilize a resonant radiofrequency (RF) field to induce an optical absorption resonance. The other two magnetometers of this type are all-optical: in Bell-Bloom magnetometers, amplitude modulation of the optical field plays the role of the effective RF interrogation, and, unlike others, this type of magnetometer can operate as an active device if the output signal of a photodetector is fed back into the modulation circuit. Finally, Hanle magnetometers use a pump-probe geometry, in which atomic spins are oriented with a circularly polarized strong pump optical field, and then their precession in the bias magnetic field is probed through the polarization rotation of a weaker probe optical field. The most successful realization of the Hanle magnetometer operates in the SERF regime, which has now become a well-recognized magnetometer type in its own right. The magnetometer operating principles in the first four columns of Table 2 may be loosely categorized under the umbrella of “magneto-optical double resonance” — a

general term which refers to the dual combination of optical and magnetic resonances, manifested physically when the frequency of an applied or effective RF field matches the Larmor frequency. This concept and its experimental demonstration in atomic spectroscopy predate magnetometry applications [118, 119].

By contrast, the devices in the last two columns of Table 2 rely on evolution of a quantum superposition of atomic spin states, rather than on magnetization. Magnetometers based on nonlinear magneto-optical rotation (NMOR) generally employ linearly polarized light to create atomic alignment (Sec. 2) — a quadrupole magnetic moment, corresponding to a coherent superposition of Zeeman sublevels — and then detect the optical polarization rotation caused by alignment evolution in the magnetic field to be measured. Typically, such measurements are done using amplitude- or phase-modulated optical fields (similar to the Bell-Bloom approach) to enable detection of nonzero magnetic fields. Finally, if atoms are prepared in a non-interacting coherent superposition of the hyperfine atomic states (usually referred to as a “dark state”) via coherent population trapping (CPT), the magnetometer uses an associated transmission resonance (electromagnetically induced transparency, or EIT) to measure the magnetic-field value.

It is important to emphasize that this list is not exhaustive and that there are no clear boundaries between different methods. Indeed, many researchers have successfully combined the characteristic features of two or more of these techniques: examples include the M_z - M_x tandem [120, 121], RF atomic magnetometers sensitive to RF magnetic fields [62, 122], magnetometers based on free spin precession [123], active self-oscillating magnetometers [93, 124], and many others. A commercial example is the QuSpin zero-field magnetometer mentioned in Table 1, which is essentially a Hanle/SERF device using a single-beam M_z -type geometry to measure transverse magnetic fields [125]. Not included in Table 2 are non-alkali atomic-magnetometer types — such as those employing the technique of parametric resonance, an established subfield of fundamental and applied magnetometry research [28–30].

4.2. Typical performance characteristics of different magnetometer types

The choice of an optimal method for magnetic-field measurements depends on the application and the expected performance. Altogether, existing atomic magnetometers span a very wide range of achievable characteristics, as shown in Fig. 5. It is easy to trace some general trends, discussed in Sec. 3: for example, more sensitive devices tend to use larger vapor cells and operate at lower bandwidth. Since a given type of magnetometer may or may not be suitable for a particular application, here we discuss some specific requirements that can be important when making the choice.

What sensitivity does my application require? Hanle magnetometers operating in the SERF regime [77] (usually just referred to as “SERF magnetometers”) are currently the most sensitive among all atom-based devices by a wide margin, reaching down to the sub-fT range — although their sensitivity may vary widely depending on the

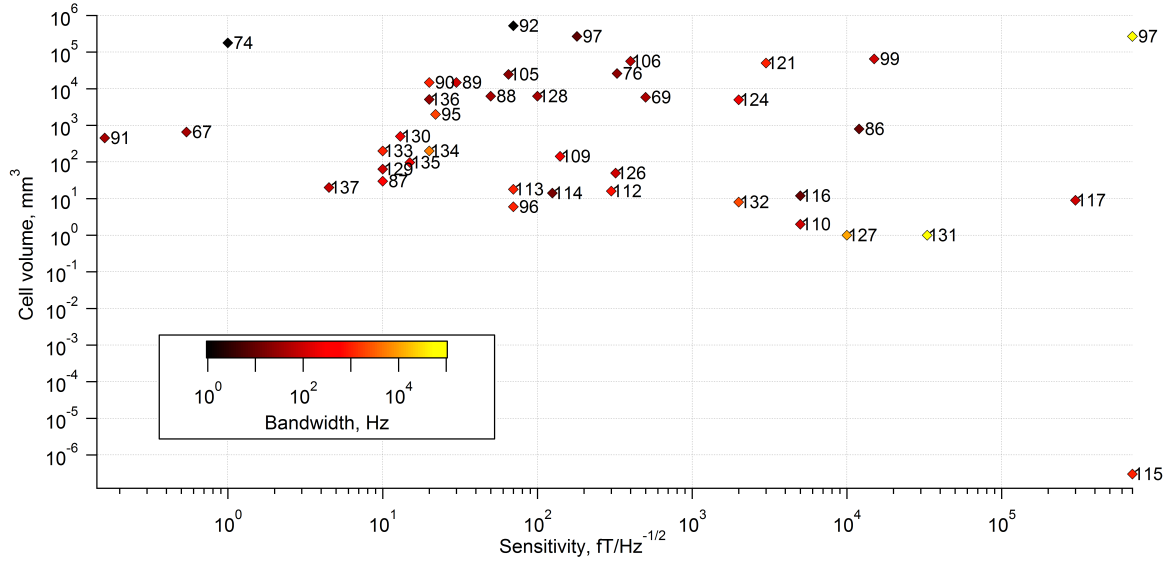


Figure 5: Characteristics of various atomic magnetometers [67, 69, 74, 76, 86–92, 95–97, 99, 105, 106, 109, 110, 112–117, 121, 124, 126–137] utilizing atomic vapor cells: magnetic-field sensitivity, cell volume, and measurement bandwidth (indicated by color).

experimental parameters, such as cell size, light-source characteristics, etc. As such, they can easily compete with SQUIDS in performance without the need for bulky cryogenics. It is important to note, however, that such magnetometers are most sensitive at zero magnetic field, and thus optimal for measuring the faintest magnetic fields in a shielded environment, such as MEG signals. In fact, the commercially available atomic magnetometers (Table 1) are primarily designed with MEG applications in mind. As discussed in Sec. 3, there is also an expected trade-off in performance, as SERF magnetometers tend to have limited dynamic range and a potentially larger volume. While these challenges can be overcome with clever engineering, for a number of applications with less stringent sensitivity requirements it may be simpler to use alternative approaches that can provide sensitivity at the level of tens of fT while operating in a fairly large background optical field (Sec. 5).

What is the expected magnetic-field magnitude? One important characteristic to consider is the base level of the measured magnetic fields. Some magnetometers (M_z/M_x , Bell-Bloom, CPT/EIT) are intrinsically designed to operate at nonzero bias magnetic field, since the measured Larmor frequency value directly appears as a frequency of the RF field or modulation. These methods are well-suited for applications in Earth’s magnetic field — for example, geomagnetometry or medical diagnostics in a magnetically unshielded environment [138]. Notably, the basic NMOR effect was also initially restricted to near-zero-field measurements, but later modifications using amplitude- or phase-modulated lasers rendered it possible to extend the operational range of NMOR-based magnetometers up to Earth field.

Which magnetic-field parameters need to be measured? Most atomic magnetometers are intrinsically **scalar**, as the measured spin-precession frequency depends only on the

magnitude of the magnetic field. However, the expected direction of the magnetic field must be taken into account even when constructing a scalar magnetometer, due to the possibility of **heading error** (the dependence of the readout on the orientation of the sensor in space) [139–141] or blind spots (the inability of the sensor to measure magnetic field in certain orientations). If information about the direction of the magnetic-field vector is required by the application, various strategies have been explored to enable operation in the **vector** modality. Most magnetometers based on the Hanle effect are intrinsically sensitive to one vector component only. Apart from that, the most common approach is to use three pairs of mutually orthogonal external magnetic-field coils to zero the magnetic field at the sensor location. In this case, the electric current in each coil can be translated into a corresponding magnetic-field component. Alternatively, the field orientation, together with the light polarization, determines the selection rules and relative strength of the involved optical transitions, and thus the vector field information may be deduced from the optical-resonance position or amplitude (or both).

How fast is the magnetic field changing? In general, speed of operation is not one of the strengths of atomic magnetometers. Their exceptional magnetic sensitivity originates from long lifetimes of atomic magnetization (Sec. 2.2), which may range from tens of milliseconds to tens of seconds depending on the size and quality of the vapor cell. However, that renders them unable to respond quickly to rapid changes in the magnetic field, limiting their operational bandwidth. Some strategies have been proposed to break this limit. For example, the operational bandwidth was successfully extended by several orders of magnitude by using active feedback to adjust the pump modulation frequency in NMOR and SERF magnetometers [97, 134], albeit with proportional deterioration of sensitivity. Alternatively, a causal waveform estimation using Kalman filtering was demonstrated to accurately predict the magnetic-field variations at time scales shorter than the sensor’s intrinsic time resolution, without paying the sensitivity penalty [142].

Can the sensor operate in a gradiometric configuration? Accurate measurements of the magnetic field using optical-atomic magnetometers may also be challenging due to a number of potential systematics, such as heading errors caused by orientation-dependent light shifts and the nonlinear Zeeman effect [139–141]. Moreover, as mentioned in Sec. 3.1, the sensitivity of measurements may be limited by technical noise from the laser or electromagnetic background coupling to the atomic spins. Some of these issues can be resolved by operating the magnetometer in gradiometer mode, in which two or more nominally identical probe regions are introduced inside the sensor to conduct differential measurements. Of course, this approach is only effective if the expected source of the magnetic field is well-localized and has a distinctly different value for each probe region. In this case, any common-mode noise will be suppressed in the differential signal, while maintaining the same useful signal. On the other hand, when it is necessary to reconstruct a detailed spatial map of the magnetic field, one must usually employ arrays of sensors [5, 23, 135, 143]. In these cases, additional system characteristics must then be considered, such as the common-mode rejection ratio, relative gain and phase stability, low crosstalk, etc., across multiple sensors.

Are there any restrictions on the physical size of the sensor? Eq. (17) clearly illustrates the advantages of larger sensor size: with a larger cell, one can increase the number of interacting atoms and reduce the magnetization decay due to collisions with the cell walls. Indeed, the best sensitivity for all types of atomic magnetometers has been demonstrated in cells with a few-cm³ volume. However, as discussed in Sec. 3.2, a large sensor size severely limits the spatial resolution as well as the achievable standoff distance. Many applications place restrictions on the sensor dimensions, unavoidably compromising their sensitivity, while also increasing the risk of magnetic-field gradients. Indeed, while most types of magnetometers have been successfully shrunk to few-mm³ cell volumes, the average sensitivity of such miniature versions dropped to a few pT/ $\sqrt{\text{Hz}}$. Notably, the magnetometers with purely optical interrogation (NMOR, EIT, Bell-Bloom) seem better suited for extreme miniaturization to chip-scale sensor sizes, whereas the need for rf coils around the cell poses additional geometrical limitations for M_z and M_x magnetometers. An alternative approach to enhancing spatial resolution in larger buffer-gas cells with low spin diffusion is to use multiple probe beams and a photodiode array, thereby subdividing the cell into multiple effective miniature sensing volumes [54]. Finally, to obtain true sub-wavelength magnetic-field resolution, nanocells can be utilized [144].

5. Choose your components and assemble your magnetometer

In Sec. 2 we derived the basic equations (15) for the zero-field resonances of a Hanle/SERF magnetometer, which was further discussed in Sec. 4. In the derivation we assumed that $\Omega_y = 0$ and $\Omega_z = 0$, which means that this kind of magnetometer works only in conditions where all components of the magnetic field are close to zero. We assumed further that the optical pumping is along the z -direction (Fig. 2). Consequently, the measurement of the M_y component must not contribute to the optical pumping and thus must rely on a measurement principle that does not involve resonant circularly polarized light. Both conditions can be achieved experimentally but typically require good magnetic shields, magnetic compensation coils in all directions, and a second laser to produce probe light. For the rest of this section, however, we mainly focus on magnetometer schemes that are easier to implement, in particular the M_z mode of operation (Table 2).

Monitoring the transmission of the laser, used for optical pumping, also allows us to measure the M_z component. While the absorptive Lorentzian line shape is perfectly suited for the optimization of the magnetometer (Sec. 5.3–5.4), it does not give us a signal proportional to the magnetic field, as was derived in Eq. (15). To obtain such a signal requires generating the derivative of the absorptive Lorentzian. This is typically achieved by applying an additional oscillating magnetic field using a coil. Figure 2B shows the setup in which a function generator drives the modulation coil with a sinusoidal current $B_m(t) = A_m \sin(\omega_m t)$. The frequency ω_m of the modulation has to be slow enough that the magnetization does not deviate significantly from its

steady state, which means that $\omega_m < \Gamma$. The derivative of the Lorentzian is generated when the signal from the photodiode is demodulated using a lock-in amplifier [145]. Internally, the lock-in determines the amplitude of the signal component at a given reference frequency, which should be the same as ω_m . The output of the lock-in (Fig. 6) is phase-sensitive: positive when the signal and the reference are in-phase and negative when they are out-of-phase. Thus, on the rising slope of the Lorentzian the output is positive and on the falling slope it is negative.

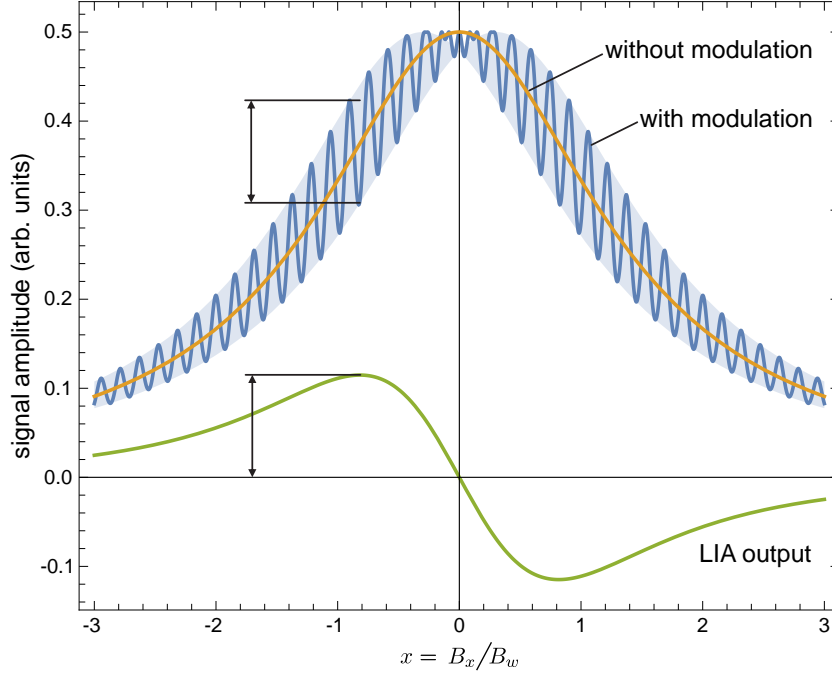


Figure 6: Generation of a dispersive signal from an absorptive signal, using a lock-in amplifier.

This is still not the full picture for an M_z magnetometer, since in general we do not measure only around $B_x = 0$, and the magnetometer can operate in an unshielded environment at Earth field (Table 2). So how can a useful absorption signal be generated? As usual, we return to the modified Bloch equation, Eq. (13), and write out the time derivatives of the magnetization components for our case:

$$\frac{d}{dt} \begin{pmatrix} M_x(t) \\ M_y(t) \\ M_z(t) \end{pmatrix} = \begin{pmatrix} M_y \Omega_z & -M_z \Omega_y & -\Gamma M_x \\ M_z \Omega_x & -M_x \Omega_z & -\Gamma M_y \\ M_x \Omega_y & -M_y \Omega_x & +\Gamma (M_a - M_z) \end{pmatrix}. \quad (21)$$

For simplicity we continue to assume that the longitudinal and transverse atomic-spin components exhibit the same relaxation behavior, i.e. $T_1 \approx T_2$ (Sec. 2.2). Solving the system of equations for the steady state, we find the longitudinal term

$$M_z = M_a \frac{\Gamma^2 + \Omega_z^2}{\Gamma^2 + \Omega_x^2 + \Omega_y^2 + \Omega_z^2}. \quad (22)$$

Thus, we see that a small amplitude change in either of the transverse fields will modulate M_z , but there is also a messy dependence on changes in the longitudinal field.

Luckily, clever tuning of the modulation coil to the Larmor frequency Ω_z generates a DC absorption dip which allows us to measure and track changes in B_z . This is best understood in the reference frame rotating around the z -axis at the Larmor frequency Ω_z . An atomic spin at rest in this rotating frame effectively experiences $B_z = 0$. If the additional field is applied along the x -direction, $B_{\text{RF}} = \sin(\omega_{\text{RF}} t)$ in the laboratory frame, it appears in the rotating frame as a static field $B_{\text{RF}} \hat{x}$ when the resonance condition $\omega_{\text{RF}} = \Omega_z$ is met. Thus, the spin will tend to rotate around \hat{x} in the y - z plane. This tipping of the spin away from \hat{z} produces a resonant dip in the absorption signal measured by the photodetector. In order to generate a dispersive signal for locking to the resonance, the oscillation frequency of the applied field can be modulated around Ω_z .

We shall now present some important aspects of magnetometer assembly, which will prepare us for discussion of actual operation in Sec. 5.4.

5.1. Choice of atomic system and vapor cell

Why do we use alkali atoms in atomic magnetometers? An alkali atom has a single valence electron, which makes it an ideal candidate for optical pumping and control of the electronic angular momentum (Sec. 2.1).

Does it matter which alkali atom I choose? In many cases, the choice of atom may be informed by strictly technical considerations such as availability of lasers at the appropriate wavelengths. Beyond that, requirements of the particular application should be considered. For example, different atomic species have different vapor pressures, with the vapor pressure of cesium being higher at any given temperature than that of rubidium, potassium, sodium, or lithium [51]. This makes cesium a popular choice for operation near room temperature [24, 62]. The frequency resolution of different isotopic and hyperfine lines in the atomic spectra also varies by atomic species, and is an important consideration for magnetometry modalities requiring such resolution. For applications requiring robustness in non-laboratory conditions, potassium is a favorite due to its narrowband spectral lines.

Should I heat my vapor cell? As discussed in Sec. 3.1, since the sensitivity of a magnetometer is ultimately limited by the number of atoms in the interaction volume (Eq. (17)), it is beneficial to increase this number as much as possible. In order to increase the atomic density without increasing the overall cell size, one typically heats the cell above room temperature. Different techniques are possible, including ovens and coil-based heating systems using high-resistance wire [146]. Care must be taken to avoid heating gradients which can damage the cells, particularly if antirelaxation coating

is used — another reason why buffer-gas cells are preferred for higher-temperature operation. Coated cells are intended to be heated to temperatures up to around 40°C, depending on the exact chemical composition of the coating used. Radiation trapping of spontaneous emission may also play a negative role at higher atomic densities, unless quenching buffer gas is introduced [147, 148].

I need a microfabricated vapor cell — what are my options? Although we saw in Sec. 3 that reducing the number of atoms worsens the sensitivity of a magnetometer, there may be strong motivations for miniaturization — including reduced standoff distance and improved spatial resolution, or integration of the cell into small quantum systems [23, 96, 111, 113–115, 149–151] with low size, weight, and power (SWaP). Production of MEMS (“micro-electromechanical systems”) vapor cells for magnetometers and atomic clocks is a rapidly growing field, typically incorporating anodic-bonding techniques [152–154]. Most MEMS vapor cells are filled with buffer gas, although antirelaxation-coated cells may offer advantages for biological applications where elevated-temperature operation is problematic [24, 155].

5.2. Laser systems and magnetic shielding

Nowadays there are a number of commercial laser systems suitable for atomic magnetometry available at various price ranges, including edge-emitting and distributed-feedback (DFB) diode lasers and vertical-cavity surface-emitting lasers (VCSELs). An inexpensive but more time-consuming option is to construct a homemade device using a laser-diode element. The main requirement in any case is single-mode operation around the alkali optical transition of interest, so frequency stabilization of the probe light is critical. (An introductory treatment of the theory of laser locking, also relevant to frequency stabilization generally, can be found in [156].) Laser power requirements may vary according to the specific magnetometer implementation; in devices utilizing two separate probe and pump beams, higher power is required for optical pumping than for probe readout.

When conducting sensitive magnetometry measurements at zero field, for example in the SERF regime, one needs to reliably shield atoms from unwanted ambient fields. Therefore the cell is contained in a nested magnetic-shielding structure, which may be small enough to fit on a laser table or large enough for experimenters to enter (magnetically shielded room [157]). The innermost layers of the shield typically contain a system of coils to produce the desired DC and/or RF magnetic fields for magnetometer operation, as well as to compensate for field gradients in the cell volume. The surrounding layers usually consist of mu-metal and iron, while strategically placed holes in the shield enable access for laser beams and cables. Mu-metal is a nickel-iron alloy with high magnetic permeability. The idea behind magnetic shielding is not actually to block external fields, but rather to provide a literal “path of least resistance” for the magnetic field lines. Since the permeability, and therefore the effectiveness, of

mu-metal varies with field strength, several layers can be used to successively reduce the unwanted fields: an outermost iron layer takes care of stronger fields, since iron saturates at a higher field strength than does mu-metal. Such tabletop shielding systems are commercially available, offering shielding factors on the order of 10^6 in the central region, or may be machined according to individual requirements. To further improve shielding performance, active compensation coils may be used, with current state-of-the-art solutions even enabling MEG measurements from human subjects in motion within shielded rooms [158].

Of course, many atomic magnetometers operate unshielded within Earth's field (typically at the cost of sensitivity performance, see Table 2), or unshielded within field-canceling coil systems [98, 103, 159]. For Earth-field operation, it may be especially desirable to operate in a gradiometric configuration [151].

5.3. Cell performance

Before being used for magnetometry or any other experiment, an atomic vapor cell must undergo a testing process in order to verify that several requirements are fulfilled:

- There are in fact atoms in the cell.
- The density of atoms is sufficiently high.
- It is possible to create a high-quality spin-polarization state (magnetization).
- The buffer-gas or coating quality (see below) is such that the decay time T_1 of the magnetization is adequately long.

Further information about how to conduct such tests may be found in various introductory references and theses covering absorption spectroscopy, optical pumping, and spin-relaxation measurements [146, 160, 161].

What is the difference between buffer-gas and antirelaxation-coated vapor cells? The smaller the magnetization relaxation rate, the longer the atomic spins can precess in the magnetic field and the more accurately the magnetic field can be measured (Sec. 3.1). While ground-state spin coherence of alkali atoms isolated from the environment can live almost indefinitely long, there are many experimental factors that limit its lifetime. Random motion of thermal atoms inside a glass cell inevitably leads to their collisions with the cell walls, which effectively destroy any prior magnetization and lead to thermalization of the atomic spin state. Thus, in an evacuated cell the effective spin relaxation rate is determined by the average time it takes for atoms to cross the laser beam (known as transient time). For a typical few-mm-wide laser beam, this time is limited to a few microseconds.

To extend the spin-relaxation time T_2 , two common strategies are employed. In one, a buffer gas is added to the cell, so that alkali atoms undergo diffusive, rather than ballistic motion. This way, the T_2 time can be significantly lengthened. The choice and pressure of the buffer gas is typically customized for each cell geometry: while

higher pressure increases atomic transient time, it also increases resonance collisional broadening and shifts [48]. Most common buffer gases are inert gases with low collisional cross-sections (Ne, He, Ar, etc.), although nitrogen (N_2) is commonly used to quench spontaneous emission. The main advantages of using cells with buffer gas are their scalability (the shorter transient time due to reduction in the cell volume can be at least partially compensated by an increase in buffer-gas pressure) and relative manufacturing simplicity. Notably, collisions with buffer gas are not always bad: a high collision rate plays a crucial role in the excellent performance of SERF magnetometers (Sec. 4), as it allows for suppression of the spin-exchange decoherence mechanism in a dense vapor [77]. At the same time, there are some potentially serious drawbacks: buffer gas effectively “freezes” atoms in their locations, making the system more susceptible to local magnetic-field gradients and inhomogeneous optical pumping. Also, collisional dephasing of the excited state is typically much more significant than for the ground state, leading to additional homogeneous broadening of optical transitions. In conjunction with velocity-changing collisions, this can result in undesirable modifications of the atomic-spin response, especially in the presence of multiple excited states [162].

The second approach is to use a hydrocarbon antirelaxation coating for the inner cell walls, which is applied during cell production. The science of antirelaxation coatings for atomic vapor cells has actually been described in the literature as “black magic”. This is because the details of how the coating works are not fully understood, and the coating process does not necessarily yield reproducible results in cell performance. Hence, for mass production of commercial systems, buffer-gas cells are typically preferred (Table 1) At the time of writing, there are no commercially available anti-relaxation coated vapor cells, although such cells are used in some commercially available magnetometers [163].

The process of alkali-atom relaxation on paraffin surfaces was modeled quantitatively, based on experimental work, already in the 1960s [65]. Some relevant qualitative points are the following. Atoms do not scatter elastically off the coated surface, but rather spent a finite time in the coating. For temperatures in the range 20–60°C, this is an adsorption process. (Adsorption is the process whereby molecules adhere to a surface; in absorption, they are taken up by a volume.) Spin relaxation takes place primarily at the walls and not in the cell body, as supported by the fact that the relaxation times scale with the cell dimensions [164].

Antirelaxation coatings are conventionally based on paraffin, also known as alkane (C_nH_{2n+2}). In recent years, coatings based on alkene (C_nH_{2n}) have also shown promise. An important parameter is the number of atom-wall collisions (bounces) that the coating can sustain before the atomic spins depolarize: on order 10^4 polarization-preserving bounces for paraffin and 10^6 for alkene [165]. Although the interaction of alkali atoms with alkene surfaces has not been studied in detail, it appears that the performance enhancement is related to carbon double bonds which are present in alkene but absent in paraffin [3]. However, paraffin coatings tend to offer better performance operation above room temperature [146]. In the SERF regime, buffer-gas cells are the only viable

choice. Further details regarding production of various coated-cell types may be found in [166, 167], and specific considerations of optical pumping in coated cells are treated in [148].

5.4. Magnetometer operation

Further technical details of setting up an atomic magnetometer in the lab may vary greatly depending on the operating mode (Sec. 4) — see, e.g. [168]. Regardless of the specific design, however, one usually needs to go through the following general steps:

- (i) Align the vapor cell and all optomechanics with respect to the laser beam(s).
- (ii) Lock each laser to the correct frequency.
- (iii) Prepare the atomic spins via optical pumping, and allow them to evolve in the presence of the magnetic field to be measured.
- (iv) Scan the magnetic resonance to obtain the magnetometer signal in frequency space (Fig. 4).
- (v) Tuning to resonance, for example via phase-locking techniques, enables tracking changes in the magnetic field as a function of time.

As mentioned previously, the linewidth of the magnetic resonance in step (iv) is proportional to the transverse coherence rate $1/T_2$, so in principle one may be able to extract the T_2 value directly from the magnetometer signal. However, the strength of optical fields affects this linewidth, so the most precise T_2 measurements are usually conducted using a pulsed pump/probe regime whereby a free-induction-decay (FID) signal can be obtained. Another common approach to finding the T_2 time is to measure power-broadened resonance linewidths and extrapolate to zero laser power [66]. Whether or not such an investigation is necessary or desirable is context-dependent; for many applications it suffices to perform characterization of magnetometer time-series data as discussed in Sec. 6. However, linewidth measurements can be an important tool for noise characterization (Sec. 3.1), as various noise sources — including magnetic-field gradients and anything else that couples to the atomic spins — manifest themselves as broadening mechanisms.

In terms of data acquisition, there is great freedom of choice as regards both hardware and software. Commercial data-acquisition (DAQ) systems are available with a corresponding price tag; lower-budget options may involve open-source software and inexpensive hardware such as a computer sound card [169]. When sampling an oscillating signal, care should be taken to ensure that the sampling rate is fast enough to avoid aliasing effects.

6. Characterize and optimize your magnetometer

To illustrate how to analyze actual data, in Appendix C we provide magnetometer time-series data from [170], along with an accompanying analysis notebook. Although the

data were obtained with a Hanle magnetometer, the illustrated analysis techniques are broadly applicable. The analysis is performed in Mathematica, but any other analysis program with similar capabilities can be used instead.

Measurement of magnetic signals in the time domain may be interesting and useful in itself, especially in the case of transient and/or triggered signals such as those encountered in biological applications. However, to characterize magnetometer performance as per the figures of merit introduced in Sec. 3, it is generally more instructive to work in the frequency domain. This is usually done by applying a fast Fourier transform (FFT) to the time-series data, in order to produce a frequency spectrum.

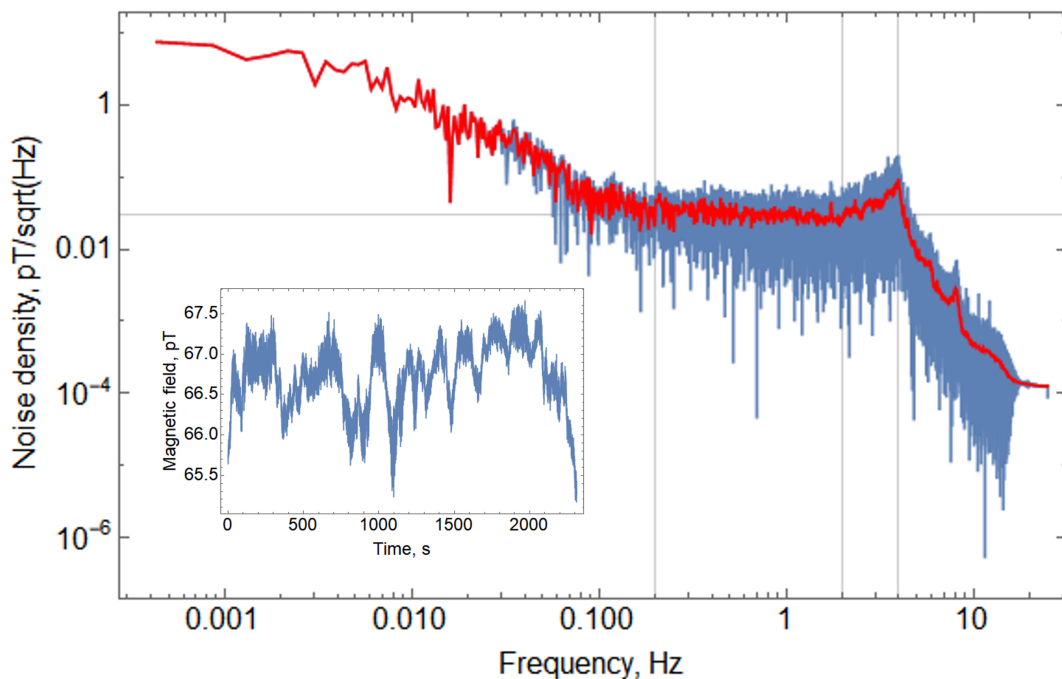


Figure 7: Noise-density frequency spectrum obtained by applying a fast Fourier transform (FFT) to raw magnetometer time-series data (inset) from [170]. The red and blue curves show the results with and without averaging, respectively. Vertical lines separate frequency regions dominated by different noise behavior, as explained in the text; the horizontal line indicates magnetometer sensitivity in the bandwidth of flat frequency response.

Fig. 7 illustrates this analysis process for the case where no magnetic signal is present, such that the intrinsic magnetometer noise can be characterized. Looking at the noise-density spectrum, we see that the noise behavior is highly frequency-dependent and can be characterized as follows:

- The noise is highest at lower frequencies, dominated by $1/f$ (so-called “pink” or “flicker”) noise from background magnetic fields.
- Between 0.2 and 2 Hz, we have the flat or “white”-noise region of the spectrum. This region defines the useful bandwidth of the magnetometer and corresponds to a sensitivity of $30 \text{ fT}/\sqrt{\text{Hz}}$.

- The noise increases between 2 and 4 Hz, in this case due to an acoustic resonance of the magnetically shielded room in which measurements were conducted.
- Above 4 Hz, the magnetometer response drops off rapidly, here because of the low-pass filter of the lock-in amplifier used for data acquisition.

For purposes of characterizing magnetometer response, data may also be obtained by measuring known magnetic-field reference signals produced using a calibrated coil system — standard procedure for device optimization before any measurement of unknown fields is attempted. Peaks should then appear in the frequency spectrum corresponding to the frequencies of the applied fields; any peaks already appearing in the absence of applied fields are likely due to frequency-dependent noise sources.

7. Typical applications of atomic magnetometers

In Table 3, we summarize the main current applications of atomic magnetometers. Not surprisingly, many of these diverse applications value high sensitivity and high accuracy at frequencies below tens of Hz. Non-invasive detection of biological magnetic signals is probably the most sought-after example, since such measurements can be carried out in a magnetically shielded environment to take maximum advantage of SERF magnetometers' exceptional sensitivity. Another important feature of atomic sensors is their negligible internal magnetic signature, making them desirable both for biomedical and surveillance applications. In summary, alkali-metal atomic magnetometers are admittedly still in their early steps toward widespread commercial success, and we may optimistically expect the emergence of new applications as fuller capabilities of atomic systems are explored in research laboratories.

Biomedical	magnetomyography (MMG) [155, 171], magnetoencephalography (MEG) [5, 89, 129, 130, 136, 172–176], (fetal) magnetocardiography (MCG and fMCG) [21, 22, 98, 128, 174, 177], magnetic-field imaging (MFI) [178] magnetic biomarkers [132, 179–182] biomagnetism of plants [183, 184] and livestock [185]
Zero-/low-field NMR	[133, 134, 149, 186–193]
Geophysics	[91, 194]
Aerospace	[108, 195]
Laser guide stars	[196]
Defense and industry	underwater surveillance [143], electromagnetic induction imaging [197–200]
Fundamental science	search for new physics beyond particle standard model [40, 82, 201–204], with comagnetometry [34, 38, 39, 72, 90] precision measurements [72, 203] <i>quantum applications</i> : squeezing-enhanced magnetometers [55–58, 60, 61], quantum non-demolition measurements of atomic spins [95, 205], quantum information [206, 207], entanglement [62]

Table 3: Common applications of atomic magnetometers.

Acknowledgments

We thank our many colleagues from the Workshop on Optically Pumped Magnetometers (WOPM) for their generous support and assistance throughout the writing process, in particular Theo Scholtes. A.F. thanks Danila Barskiy, Dmitry Budker, Pavel Fadeev, Till Lenz, and Hendrik Bekker for helpful discussion and editing. Some portions of the text were adapted from [208].

References

- [1] Dmitry Budker and Michael Romalis. “Optical magnetometry”. In: *Nature Physics* 3.4 (Apr. 2007), pp. 227–234. ISSN: 17452481. DOI: 10.1038/nphys566. URL: <https://www.nature.com/articles/nphys566>.
- [2] Evgenii B. Aleksandrov and Anton K. Vershovskii. “Modern radio-optical methods in quantum magnetometry”. In: *Physics-Uspekhi* 52.6 (June 2009), pp. 573–601. ISSN: 1063-7869. URL: <https://iopscience.iop.org/article/10.3367/UFNe.0179.200906f.0605>.
- [3] Dmitry Budker and Derek F. Jackson Kimball, eds. *Optical Magnetometry*. Cambridge: Cambridge University Press, May 2013. ISBN: 9780511846380. DOI: 10.1017/CB09780511846380. URL: <http://ebooks.cambridge.org/ref/id/CB09780511846380>.
- [4] Antoine Weis, Georg Bison, and Zoran D. Grujić. “Magnetic resonance based atomic magnetometers”. In: *High Sensitivity Magnetometers. Smart Sensors, Measurement and Instrumentation*. Ed. by A. Grosz, M. Haji-Sheikh, and S. Mukhopadhyay. Vol. 19. Cham: Springer, 2017, pp. 361–424. ISBN: 978-3-319-34068-5. DOI: 10.1007/978-3-319-34070-8. URL: https://link.springer.com/chapter/10.1007/978-3-319-34070-8_13.
- [5] Tim M. Tierney et al. “Optically pumped magnetometers: From quantum origins to multi-channel magnetoencephalography”. In: *NeuroImage* 199 (Oct. 2019), pp. 598–608. ISSN: 10959572. DOI: 10.1016/j.neuroimage.2019.05.063. URL: <https://www.sciencedirect.com/science/article/pii/S1053811919304550>.
- [6] Kai Mei C. Fu et al. “Sensitive magnetometry in challenging environments”. In: *AVS Quantum Science* 2.4 (Dec. 2020), p. 044702. ISSN: 26390213. DOI: 10.1116/5.0025186. URL: <https://avs.scitation.org/doi/abs/10.1116/5.0025186>.
- [7] Michael V. Romalis. “Optically pumped magnetometers for biomagnetic measurements”. In: *Flexible High Performance Magnetic Field Sensors*. Ed. by Etienne Labyt, Tilmann Sander, and Ronald Wakai. Cham: Springer, 2022, pp. 3–15. ISBN: 978-3-031-05362-7. DOI: 10.1007/978-3-031-05363-4. URL: https://link.springer.com/chapter/10.1007/978-3-031-05363-4_1.
- [8] Roswitha Wiltschko, Christine Nießner, and Wolfgang Wiltschko. “The magnetic compass of birds: The role of cryptochrome”. In: *Frontiers in Physiology* 12 (May 2021), p. 667000. ISSN: 1664042X. DOI: 10.3389/fphys.2021.667000. URL: <https://www.frontiersin.org/articles/10.3389/fphys.2021.667000/full>.
- [9] Jingjing Xu et al. “Magnetic sensitivity of cryptochrome 4 from a migratory songbird”. In: *Nature* 594.7864 (June 2021), pp. 535–540. ISSN: 1476-4687. DOI: 10.1038/s41586-021-03618-9. URL: <https://www.nature.com/articles/s41586-021-03618-9>.

- [10] James L. Gould. “Animal navigation: The evolution of magnetic orientation”. In: *Current Biology* 18.11 (June 2008), R482–R484. ISSN: 09609822. DOI: 10.1016/j.cub.2008.03.052. URL: [https://www.cell.com/current-biology/fulltext/S0960-9822\(08\)00394-1](https://www.cell.com/current-biology/fulltext/S0960-9822(08)00394-1).
- [11] Hans Aschenbrenner and Georg Goubau. “Eine Anordnung zur Registrierung rascher Magnetischer Störungen”. In: *Hochfreq. Electroakustik* 47.6 (1936), pp. 177–181.
- [12] Michal Janosek. “Parallel fluxgate magnetometers”. In: *High Sensitivity Magnetometers. Smart Sensors, Measurement and Instrumentation*. Ed. by A. Grosz, M. Haji-Sheikh, and S. Mukhopadhyay. Vol. 19. Cham: Springer, 2017, pp. 41–61. ISBN: 978-3-319-34068-5. DOI: 10.1007/978-3-319-34070-8. URL: https://link.springer.com/chapter/10.1007/978-3-319-34070-8_2.
- [13] Nikolay Koshev et al. “Evolution of MEG: A first MEG-feasible fluxgate magnetometer”. In: *Human Brain Mapping* 42.15 (Oct. 2021), pp. 4844–4856. ISSN: 10970193. DOI: 10.1002/hbm.25582. URL: <https://onlinelibrary.wiley.com/doi/10.1002/hbm.25582>.
- [14] G. S. Waters and P. D. Francis. “A nuclear magnetometer”. In: *Journal of Scientific Instruments* 35.3 (Mar. 1958), pp. 88–93. ISSN: 09507671. DOI: 10.1088/0950-7671/35/3/302. URL: <https://iopscience.iop.org/article/10.1088/0950-7671/35/3/302>.
- [15] Arnold L. Bloom. “Principles of operation of the rubidium vapor magnetometer”. In: *Applied Optics* 1.1 (Jan. 1962), p. 61. ISSN: 0003-6935. DOI: 10.1364/ao.1.000061. URL: <https://www.osapublishing.org/ao/abstract.cfm?uri=ao-1-1-61>.
- [16] R. C. Jaklevic et al. “Quantum interference effects in Josephson tunneling”. In: *Physical Review Letters* 12.7 (Feb. 1964), pp. 159–160. ISSN: 00319007. DOI: 10.1103/PhysRevLett.12.159. URL: <https://journals.aps.org/prl/abstract/10.1103/PhysRevLett.12.159>.
- [17] C. N. Owston. “A Hall effect magnetometer for small magnetic fields”. In: *Journal of Scientific Instruments* 44.9 (Sept. 1967), pp. 798–800. ISSN: 09507671. DOI: 10.1088/0950-7671/44/9/441. URL: <https://iopscience.iop.org/article/10.1088/0950-7671/44/9/441>.
- [18] H. Hoffmann, F. Hofmann, and W. Schoepe. “Magnetoresistance and non-Ohmic conductivity of thin platinum films at low temperatures”. In: *Physical Review B* 25.8 (Apr. 1982), pp. 5563–5565. ISSN: 01631829. DOI: 10.1103/PhysRevB.25.5563. URL: <https://journals.aps.org/prb/abstract/10.1103/PhysRevB.25.5563>.
- [19] Asaf Grosz, Michael J. Haji-Sheikh, and Subhas C. Mukhopadhyay, eds. *High Sensitivity Magnetometers*. Vol. 19. Smart Sensors, Measurement and Instrumentation. Cham, Switzerland: Springer International Publishing, 2017. ISBN: 9783319340685. DOI: 10.1007/978-3-319-34070-8. URL: <http://link.springer.com/10.1007/978-3-319-34070-8>.
- [20] Kasper Jensen, Pauli Kehayias, and Dmitry Budker. “Magnetometry with nitrogen-vacancy centers in diamond”. In: *High Sensitivity Magnetometers. Smart Sensors, Measurement and Instrumentation*. Ed. by A. Grosz, M. Haji-Sheikh, and S. Mukhopadhyay. Vol. 19. Cham: Springer, 2017, pp. 553–576. ISBN: 978-3-319-34068-5. DOI: 10.1007/978-3-319-34070-8. URL: https://link.springer.com/chapter/10.1007/978-3-319-34070-8_18.

- [21] Tilmann Sander et al. “Optically pumped magnetometers enable a new level of biomagnetic measurements”. In: *Advanced Optical Technologies* 9.5 (Oct. 2020), pp. 247–251. ISSN: 21928584. DOI: 10.1515/aot-2020-0027. URL: <https://www.degruyter.com/document/doi/10.1515/aot-2020-0027/html>.
- [22] Margo Batie et al. “Detection of fetal arrhythmia by using optically pumped magnetometers”. In: *JACC: Clinical Electrophysiology* 4.2 (Feb. 2018), pp. 284–287. ISSN: 2405500X. DOI: 10.1016/j.jacep.2017.08.009. URL: <https://www.ncbi.nlm.nih.gov/pmc/articles/PMC5841248>.
- [23] N. V. Nardelli et al. “A conformal array of microfabricated optically-pumped first-order gradiometers for magnetoencephalography”. In: *EPJ Quantum Technology* 7.1 (Sept. 2020), pp. 1–11. ISSN: 21960763. DOI: 10.1140/epjqt/s40507-020-00086-4. URL: <https://epjquantumtechnology.springeropen.com/articles/10.1140/epjqt/s40507-020-00086-4>.
- [24] Kasper Jensen et al. “Magnetocardiography on an isolated animal heart with a room-temperature optically pumped magnetometer”. In: *Scientific Reports* 8.1 (Nov. 2018), pp. 1–9. ISSN: 20452322. DOI: 10.1038/s41598-018-34535-z. URL: <https://www.nature.com/articles/s41598-018-34535-z>.
- [25] W. Gawlik and J. M. Higbie. “Magnetometry with cold atoms”. In: *Optical Magnetometry*. Ed. by Dmitry Budker and Derek F. Jackson Kimball. Cambridge University Press, May 2013. Chap. 9, pp. 167–189. ISBN: 9780511846380. DOI: 10.1017/CB09780511846380.010. URL: <https://www.cambridge.org/core/books/optical-magnetometry/magnetometry-with-cold-atoms/AE8C14285BFF2E77508641AFCABC47A9>.
- [26] Yuval Cohen et al. “A cold atom radio-frequency magnetometer”. In: *Applied Physics Letters* 114.7 (Feb. 2019), p. 073505. ISSN: 00036951. DOI: 10.1063/1.5084004. URL: <https://aip.scitation.org/doi/abs/10.1063/1.5084004>.
- [27] Werner Heil. “Helium magnetometers”. In: *High Sensitivity Magnetometers. Smart Sensors, Measurement and Instrumentation*. Ed. by A. Grosz, M. Haji-Sheikh, and S. Mukhopadhyay. Vol. 19. Cham: Springer, 2017, pp. 493–521. ISBN: 978-3-319-34068-5. DOI: 10.1007/978-3-319-34070-8. URL: https://link.springer.com/chapter/10.1007/978-3-319-34070-8_16.
- [28] William Fourcault et al. “Helium-4 magnetometers for room-temperature biomedical imaging: toward collective operation and photon-noise limited sensitivity”. In: *Optics Express* 29.10 (May 2021), p. 14467. ISSN: 10944087. DOI: 10.1364/oe.420031. URL: <https://opg.optica.org/oe/fulltext.cfm?uri=oe-29-10-14467&id=450547>.
- [29] F. Bertrand et al. “A 4He vector zero-field optically pumped magnetometer operated in the Earth-field”. In: *Review of Scientific Instruments* 92.10 (Oct. 2021), p. 105005. ISSN: 10897623. DOI: 10.1063/5.0062791. URL: <https://aip.scitation.org/doi/abs/10.1063/5.0062791>.
- [30] Gwenaél Le Gal, Laure Line Rouve, and Agustin Palacios-Laloy. “Parametric resonance magnetometer based on elliptically polarized light yielding three-axis measurement with isotropic sensitivity”. In: *Applied Physics Letters* 118.25 (June 2021), p. 254001. ISSN: 00036951. DOI: 10.1063/5.0047124. URL: <https://aip.scitation.org/doi/abs/10.1063/5.0047124>.

- [31] Jean Michel Léger et al. “In-flight performance of the Absolute Scalar Magnetometer vector mode on board the Swarm satellites”. In: *Earth, Planets and Space* 67.1 (Apr. 2015), pp. 1–12. ISSN: 18805981. DOI: 10.1186/s40623-015-0231-1. URL: <https://earth-planets-space.springeropen.com/articles/10.1186/s40623-015-0231-1>.
- [32] A. Maul et al. “Nuclear hyperpolarization of He 3 by magnetized plasmas”. In: *Physical Review A* 98.6 (Dec. 2018), p. 063405. ISSN: 24699934. DOI: 10.1103/PhysRevA.98.063405. URL: <https://journals.aps.org/pr/abstract/10.1103/PhysRevA.98.063405>.
- [33] Anna Nikiel et al. “Ultrasensitive ^3He magnetometer for measurements of high magnetic fields”. In: *European Physical Journal D* 68.11 (Nov. 2014), pp. 1–12. ISSN: 14346079. DOI: 10.1140/epjd/e2014-50401-3. URL: <https://link.springer.com/article/10.1140/epjd/e2014-50401-3>.
- [34] M. E. Limes, D. Sheng, and M. V. Romalis. “ ^3He - ^{129}Xe comagnetometry using ^{87}Rb detection and decoupling”. In: *Physical Review Letters* 120.3 (Jan. 2018), p. 033401. ISSN: 10797114. DOI: 10.1103/PhysRevLett.120.033401. URL: <https://journals.aps.org/prl/abstract/10.1103/PhysRevLett.120.033401>.
- [35] Min Jiang et al. “Floquet maser”. In: *Science Advances* 7.8 (Feb. 2021), pp. 719–736. ISSN: 23752548. DOI: 10.1126/sciadv.abe0719. URL: <https://www.science.org/doi/abs/10.1126/sciadv.abe0719>.
- [36] A. Palacios-Laloy, M. Le Prado, and E. Labyt. “Tri-axial helium-4 optically pumped magnetometers for MEG”. In: *Flexible High Performance Magnetic Field Sensors*. Springer, Cham, 2022, pp. 79–110. DOI: 10.1007/978-3-031-05363-4. URL: https://link.springer.com/chapter/10.1007/978-3-031-05363-4_6.
- [37] Sun Yool Park. *Construction of a Single Beam SERF Magnetometer using Potassium Atoms for GNOME - Bachelor thesis, Oberlin College*. Oberlin, OH, USA, Apr. 2019.
- [38] W. A. Terrano and M. V. Romalis. “Comagnetometer probes of dark matter and new physics”. In: *Quantum Science and Technology* 7.1 (Nov. 2022), p. 014001. ISSN: 20589565. DOI: 10.1088/2058-9565/ac1ae0. URL: <https://iopscience.iop.org/article/10.1088/2058-9565/ac1ae0>.
- [39] Mikhail Padniuk et al. “Response of atomic spin-based sensors to magnetic and nonmagnetic perturbations”. In: *Scientific Reports* 2022 12:1 12.1 (Jan. 2022), pp. 1–9. ISSN: 2045-2322. DOI: 10.1038/s41598-021-03609-w. URL: <https://www.nature.com/articles/s41598-021-03609-w>.
- [40] Haowen Su et al. “Search for exotic spin-dependent interactions with a spin-based amplifier”. In: *Science Advances* 7.47 (Nov. 2021), p. 9535. ISSN: 23752548. DOI: 10.1126/sciadv.abi9535. URL: <https://www.science.org/doi/full/10.1126/sciadv.abi9535>.
- [41] Dmitry Budker, Derek F. Kimball, and David P. Demille. *Atomic Physics: An Exploration Through Problems and Solutions*. 2nd ed. 3. Oxford University Press, July 2008. ISBN: 9780199532414. URL: <https://global.oup.com/academic/product/atomic-physics-9780199532414>.
- [42] Marcis Auzinsh, Dmitry Budker, and Simon Rochester. *Optically Polarized Atoms: Understanding Light-Atom Interactions*. 10. Oxford University Press, July 2010. ISBN: 9780199565122. URL: <https://global.oup.com/academic/product/optically-polarized-atoms-9780199565122>.

- [43] Hans Marin Florez and Tadas Pyragius. “Floquet description of optically pumped magnetometers”. In: *Physical Review A* 103.3 (Mar. 2021), p. 033113. ISSN: 2469-9926. DOI: 10.1103/PhysRevA.103.033113. URL: <https://link.aps.org/doi/10.1103/PhysRevA.103.033113>.
- [44] Brian Julsgaard. “Entanglement and Quantum Interactions with Macroscopic Gas Samples”. PhD thesis. Aarhus, Denmark: Center for Quantum Optics (QUANTOP), Oct. 2003.
- [45] C. Cohen-Tannoudji et al. “Detection of the static magnetic field produced by the oriented nuclei of optically pumped ^3He gas”. In: *Physical Review Letters* 22.15 (Apr. 1969), p. 758. ISSN: 00319007. DOI: 10.1103/PhysRevLett.22.758. URL: <https://journals.aps.org/prl/abstract/10.1103/PhysRevLett.22.758>.
- [46] G. G. Scott. “Review of gyromagnetic ratio experiments”. In: *Reviews of Modern Physics* 34.1 (Jan. 1962), p. 102. ISSN: 00346861. DOI: 10.1103/RevModPhys.34.102. URL: <https://journals.aps.org/rmp/abstract/10.1103/RevModPhys.34.102>.
- [47] S. M. Rochester et al. “Orientation-to-alignment conversion and spin squeezing”. In: *Physical Review A - Atomic, Molecular, and Optical Physics* 85.2 (Feb. 2012), p. 022125. ISSN: 10502947. DOI: 10.1103/PhysRevA.85.022125. URL: <https://journals.aps.org/pra/abstract/10.1103/PhysRevA.85.022125>.
- [48] William Happer. “Optical pumping”. In: *Reviews of Modern Physics* 44.2 (Apr. 1972), pp. 169–249. ISSN: 00346861. DOI: 10.1103/RevModPhys.44.169. URL: <https://journals.aps.org/rmp/abstract/10.1103/RevModPhys.44.169>.
- [49] M. Auzinsh et al. “F -resolved magneto-optical resonances in the D1 excitation of cesium: Experiment and theory”. In: *Physical Review A - Atomic, Molecular, and Optical Physics* 78.1 (July 2008), p. 013417. ISSN: 10502947. DOI: 10.1103/PhysRevA.78.013417. URL: <https://journals.aps.org/pra/abstract/10.1103/PhysRevA.78.013417>.
- [50] Alexander Pouliot et al. “Investigations of optical pumping for magnetometry using an auto-locking laser system”. In: *Proc. SPIE 10637, Laser Technology for Defense and Security XIV* 10637 (May 2018), pp. 40–47. ISSN: 1996756X. DOI: 10.1117/12.2304598. URL: <https://www.spiedigitallibrary.org/conference-proceedings-of-spie/10637/106370A/Investigations-of-optical-pumping-for-magnetometry-using-an-auto-locking/10.1117/12.2304598.full>.
- [51] Daniel A. Steck. *Alkali D Line Data*. 2021. URL: <https://steck.us/alkalidata/>.
- [52] Karl Blum. *Density Matrix Theory and Applications*. Vol. 64. Springer Series on Atomic, Optical, and Plasma Physics. Berlin, Heidelberg: Springer Berlin Heidelberg, 2012. ISBN: 978-3-642-20560-6. DOI: 10.1007/978-3-642-20561-3. URL: <http://link.springer.com/10.1007/978-3-642-20561-3>.
- [53] Peter W. Milonni and Joseph H. Eberly. *Laser Physics*. Hoboken, NJ, USA: John Wiley & Sons, Inc., Mar. 2010. ISBN: 9780470387719. DOI: 10.1002/9780470409718. URL: <https://onlinelibrary.wiley.com/doi/book/10.1002/9780470409718>.
- [54] I. K. Kominis et al. “A subfemtotesla multichannel atomic magnetometer”. In: *Nature* 2003 422:6932 422.6932 (Apr. 2003), pp. 596–599. ISSN: 1476-4687. DOI: 10.1038/nature01484. URL: <https://www.nature.com/articles/nature01484>.

- [55] A. Kuzmich, Klaus Mølmer, and E. S. Polzik. “Spin squeezing in an ensemble of atoms illuminated with squeezed light”. In: *Physical Review Letters* 79.24 (Dec. 1997), pp. 4782–4785. ISSN: 10797114. DOI: 10.1103/PhysRevLett.79.4782. URL: <https://journals.aps.org/prl/abstract/10.1103/PhysRevLett.79.4782>.
- [56] M. Auzinsh et al. “Can a quantum nondemolition measurement improve the sensitivity of an atomic magnetometer?”. In: *Physical Review Letters* 93.17 (Oct. 2004), p. 173002. ISSN: 00319007. DOI: 10.1103/PhysRevLett.93.173002. URL: <https://journals.aps.org/prl/abstract/10.1103/PhysRevLett.93.173002>.
- [57] Florian Wolfgramm et al. “Squeezed-light optical magnetometry”. In: *Physical Review Letters* 105.5 (July 2010), p. 053601. ISSN: 00319007. DOI: 10.1103/PhysRevLett.105.053601. URL: <https://journals.aps.org/prl/abstract/10.1103/PhysRevLett.105.053601>.
- [58] R. J. Sewell et al. “Magnetic sensitivity beyond the projection noise limit by spin squeezing”. In: *Physical Review Letters* 109.25 (Dec. 2012), p. 253605. ISSN: 00319007. DOI: 10.1103/PhysRevLett.109.253605. URL: <https://journals.aps.org/prl/abstract/10.1103/PhysRevLett.109.253605>.
- [59] Travis Horrom et al. “Quantum-enhanced magnetometer with low-frequency squeezing”. In: *Physical Review A - Atomic, Molecular, and Optical Physics* 86.2 (Aug. 2012), p. 023803. ISSN: 10502947. DOI: 10.1103/PhysRevA.86.023803. URL: <https://journals.aps.org/prl/abstract/10.1103/PhysRevA.86.023803>.
- [60] C. Troullinou et al. “Squeezed-light enhancement and backaction evasion in a high sensitivity optically pumped magnetometer”. In: *Physical Review Letters* 127.19 (Nov. 2021), p. 193601. ISSN: 10797114. DOI: 10.1103/PhysRevLett.127.193601. URL: <https://journals.aps.org/prl/abstract/10.1103/PhysRevLett.127.193601>.
- [61] Jiahui Li and Irina Novikova. “Improving sensitivity of an amplitude-modulated magneto-optical atomic magnetometer using squeezed light”. In: *arXiv* (July 2022). DOI: 10.48550/arxiv.2207.12962. URL: <https://arxiv.org/abs/2207.12962v1>.
- [62] W. Wasilewski et al. “Quantum noise limited and entanglement-assisted magnetometry”. In: *Physical Review Letters* 104.13 (Mar. 2010), p. 133601. ISSN: 00319007. DOI: 10.1103/PhysRevLett.104.133601. URL: <https://journals.aps.org/prl/abstract/10.1103/PhysRevLett.104.133601>.
- [63] G. Vasilakis, V. Shah, and M. V. Romalis. “Stroboscopic backaction evasion in a dense alkali-metal vapor”. In: *Physical Review Letters* 106.14 (Apr. 2011), p. 143601. ISSN: 00319007. DOI: 10.1103/PhysRevLett.106.143601. URL: <https://journals.aps.org/prl/abstract/10.1103/PhysRevLett.106.143601>.
- [64] Mark Fox. *Quantum Optics: An Introduction*. Oxford University Press, Apr. 2006. ISBN: 9780198566724. URL: <https://global.oup.com/academic/product/quantum-optics-9780198566724>.
- [65] M. A. Bouchiat and J. Brossel. “Relaxation of optically pumped rb atoms on paraffin-coated walls”. In: *Physical Review* 147.1 (July 1966), pp. 41–54. ISSN: 0031899X. DOI: 10.1103/PhysRev.147.41. URL: <https://journals.aps.org/pr/abstract/10.1103/PhysRev.147.41>.
- [66] Theo Scholtes et al. “Intrinsic relaxation rates of polarized Cs vapor in miniaturized cells”. In: *Applied Physics B: Lasers and Optics* 117.1 (Oct. 2014), pp. 211–218. ISSN: 09462171. DOI: 10.1007/S00340-014-5824-z. URL: <https://link.springer.com/article/10.1007/s00340-014-5824-z>.

- [67] D. Sheng et al. “Subfemtotesla scalar atomic magnetometry using multipass cells”. In: *Physical Review Letters* 110.16 (Apr. 2013), p. 160802. ISSN: 00319007. DOI: <https://doi.org/10.1103/PhysRevLett.110.160802>. URL: <https://journals.aps.org/prl/abstract/10.1103/PhysRevLett.110.160802>.
- [68] G. Vasilakis et al. “Cavity enhanced quantum limited magnetometry”. In: *Research in Optical Sciences (2014), paper QTu3B.6* (Mar. 2014), QTu3B.6. ISSN: 21622701. DOI: 10.1364/QIM.2014.QU3B.6. URL: <https://opg.optica.org/abstract.cfm?uri=QIM-2014-QU3B.6>.
- [69] B. Cai et al. “Herriott-cavity-assisted all-optical atomic vector magnetometer”. In: *Physical Review A* 101.5 (May 2020), p. 053436. ISSN: 24699934. DOI: 10.1103/PhysRevA.101.053436. URL: <https://journals.aps.org/pra/abstract/10.1103/PhysRevA.101.053436>.
- [70] V. G. Lucivero et al. “Femtotesla direct magnetic gradiometer using a single multipass cell”. In: *Physical Review Applied* 15.1 (Jan. 2021), p. 014004. ISSN: 23317019. DOI: 10.1103/PhysRevApplied.15.014004. URL: <https://journals.aps.org/prapplied/abstract/10.1103/PhysRevApplied.15.014004>.
- [71] David W. Allan. *Allan Variance – Overview by David W. Allan*. URL: <http://www.allanstime.com/AllanVariance/index.html>.
- [72] Jason Mora et al. “Measurement of the ratio between g-factors of the ground states of 87Rb and 85Rb”. In: *Annalen der Physik* 531.5 (May 2019), p. 1800281. ISSN: 15213889. DOI: 10.1002/andp.201800281. URL: <https://onlinelibrary.wiley.com/doi/10.1002/andp.201800281>.
- [73] Evgeny B. Alexandrov. “Optically pumped atomic magnetometers after three decades”. In: *Optical Engineering* 31.4 (Apr. 1992), p. 711. ISSN: 00913286. DOI: 10.1117/12.56132. URL: <https://www.spiedigitallibrary.org/journals/optical-engineering/volume-31/issue-4/0000/Optically-pumped-atomic-magnetometers-after-three-decades/10.1117/12.56132.short>.
- [74] S. Groeger et al. “A high-sensitivity laser-pumped Mx magnetometer”. In: *European Physical Journal D* 38.2 (Feb. 2006), pp. 239–247. ISSN: 14346060. DOI: 10.1140/epjd/e2006-00037-y. URL: <https://link.springer.com/article/10.1140/epjd/e2006-00037-y>.
- [75] E. B. Aleksandrov et al. “Laser pumping in the scheme of an Mx-magnetometer”. In: *Optics and Spectroscopy (English translation of Optika i Spektroskopiya)* 78.2 (1995), pp. 292–298. ISSN: 0030400X. URL: <https://ui.adsabs.harvard.edu/abs/1995OptSp..78..292A/abstract>.
- [76] Valentina Tiporlini and Kamal Alameh. “High sensitivity optically pumped quantum magnetometer”. In: *The Scientific World Journal* 2013 (2013). ISSN: 1537744X. DOI: 10.1155/2013/858379. URL: <https://www.hindawi.com/journals/tswj/2013/858379>.
- [77] J. C. Allred et al. “High-sensitivity atomic magnetometer unaffected by spin-exchange relaxation”. In: *Physical Review Letters* 89.13 (Sept. 2002), pp. 1308011–1308014. ISSN: 00319007. DOI: 10.1103/physrevlett.89.130801. URL: <https://journals.aps.org/prl/abstract/10.1103/PhysRevLett.89.130801>.

- [78] William E. Bell and Arnold L. Bloom. “Optically driven spin precession”. In: *Physical Review Letters* 6.6 (Mar. 1961), pp. 280–281. ISSN: 00319007. DOI: 10.1103/PhysRevLett.6.280. URL: <https://journals.aps.org/prl/abstract/10.1103/PhysRevLett.6.280>.
- [79] Jundi Li et al. “SERF atomic magnetometer - Recent advances and applications: A review”. In: *IEEE Sensors Journal* 18.20 (Oct. 2018), pp. 8198–8207. ISSN: 1530437X. DOI: 10.1109/JSEN.2018.2863707. URL: <https://ieeexplore.ieee.org/document/8425967>.
- [80] D. Budker et al. “Sensitive magnetometry based on nonlinear magneto-optical rotation”. In: *Physical Review A - Atomic, Molecular, and Optical Physics* 62.4 (Sept. 2000), p. 7. ISSN: 10941622. DOI: 10.1103/PhysRevA.62.043403. URL: <https://journals.aps.org/pra/abstract/10.1103/PhysRevA.62.043403>.
- [81] D. Budker et al. “Resonant nonlinear magneto-optical effects in atoms”. In: *Reviews of Modern Physics* 74.4 (Nov. 2002), pp. 1153–1201. ISSN: 00346861. DOI: 10.1103/RevModPhys.74.1153. URL: <https://journals.aps.org/rmp/abstract/10.1103/RevModPhys.74.1153>.
- [82] M. Rosner et al. “A highly drift-stable atomic magnetometer for fundamental physics experiments”. In: *Applied Physics Letters* 120.16 (Apr. 2022), p. 161102. ISSN: 0003-6951. DOI: 10.1063/5.0083854. URL: <https://aip.scitation.org/doi/abs/10.1063/5.0083854>.
- [83] D. Budker et al. “Nonlinear magneto-optical rotation with frequency-modulated light”. In: *Physical Review A - Atomic, Molecular, and Optical Physics* 65.5 (May 2002), p. 4. ISSN: 10941622. DOI: 10.1103/PhysRevA.65.055403. URL: <https://journals.aps.org/pra/abstract/10.1103/PhysRevA.65.055403>.
- [84] W. Gawlik et al. “Nonlinear magneto-optical rotation with amplitude modulated light”. In: *Applied Physics Letters* 88.13 (Mar. 2006), p. 131108. ISSN: 0003-6951. DOI: 10.1063/1.2190457. URL: <https://aip.scitation.org/doi/abs/10.1063/1.2190457>.
- [85] A. Nagel et al. “Experimental realization of coherent dark-state magnetometers”. In: *Europhysics Letters* 44.1 (Oct. 1998), pp. 31–36. ISSN: 02955075. DOI: 10.1209/epl/i1998-00430-0. URL: <https://epljournal.edpsciences.org/articles/epl/abs/1998/19/44106/44106.html>.
- [86] M. Stähler et al. “Picotesla magnetometry with coherent dark states”. In: *Europhysics Letters* 54.3 (May 2001), pp. 323–328. ISSN: 02955075. DOI: 10.1209/epl/i2001-00245-y. URL: <https://epljournal.edpsciences.org/articles/epl/abs/2001/09/6509/6509.html>.
- [87] Volkmar Schultze et al. “An optically pumped magnetometer working in the light-shift dispersed Mz mode”. In: *Sensors (Switzerland)* 17.3 (Mar. 2017), p. 561. ISSN: 14248220. DOI: 10.3390/s17030561. URL: <https://www.mdpi.com/1424-8220/17/3/561>.
- [88] Giuseppe Bevilacqua et al. “Self-adaptive loop for external-disturbance reduction in a differential measurement setup”. In: *Physical Review Applied* 11.1 (Jan. 2019), p. 014029. ISSN: 23317019. DOI: 10.1103/PhysRevApplied.11.014029. URL: <https://journals.aps.org/prapplied/abstract/10.1103/PhysRevApplied.11.014029>.
- [89] Rui Zhang et al. “Recording brain activities in unshielded Earth’s field with optically pumped atomic magnetometers”. In: *Science Advances* 6.24 (June 2020), pp. 8792–8804. ISSN: 23752548. DOI: 10.1126/sciadv.aba8792. URL: <https://www.science.org/doi/full/10.1126/sciadv.aba8792>.

- [90] Yucheng Yang et al. “All-optical single-species cesium atomic comagnetometer with optical free induction decay detection”. In: *Applied Physics B: Lasers and Optics* 127.3 (Mar. 2021), pp. 1–11. ISSN: 09462171. DOI: 10.1007/s00340-021-07594-w. URL: <https://link.springer.com/article/10.1007/s00340-021-07594-w>.
- [91] H. B. Dang, A. C. Maloof, and M. V. Romalis. “Ultrahigh sensitivity magnetic field and magnetization measurements with an atomic magnetometer”. In: *Applied Physics Letters* 97.15 (Oct. 2010), p. 151110. ISSN: 00036951. DOI: 10.1063/1.3491215. URL: <https://aip.scitation.org/doi/abs/10.1063/1.3491215>.
- [92] Vito Giovanni Lucivero et al. “Shot-noise-limited magnetometer with sub-picotesla sensitivity at room temperature”. In: *Review of Scientific Instruments* 85.11 (Nov. 2014), p. 113108. ISSN: 10897623. DOI: 10.1063/1.4901588. URL: <https://aip.scitation.org/doi/abs/10.1063/1.4901588>.
- [93] Andrey B. Matsko, Dmitry Strekalov, and Lute Maleki. “Magnetometer based on the opto-electronic microwave oscillator”. In: *Optics Communications* 247.1-3 (Mar. 2005), pp. 141–148. ISSN: 00304018. DOI: 10.1016/j.optcom.2004.11.047. URL: <https://www.sciencedirect.com/science/article/abs/pii/S0030401804011757>.
- [94] S. Groeger et al. “Laser-pumped cesium magnetometers for high-resolution medical and fundamental research”. In: *Sensors and Actuators, A: Physical* 129.1-2 SPEC. ISS. (May 2006), pp. 1–5. ISSN: 09244247. DOI: 10.1016/j.sna.2005.09.036.
- [95] V. Shah, G. Vasilakis, and M. V. Romalis. “High bandwidth atomic magnetometry with continuous quantum nondemolition measurements”. In: *Physical Review Letters* 104.1 (Jan. 2010), p. 013601. ISSN: 00319007. DOI: 10.1103/PhysRevLett.104.013601. URL: <https://journals.aps.org/prl/abstract/10.1103/PhysRevLett.104.013601>.
- [96] Vishal Shah et al. “Subpicotesla atomic magnetometry with a microfabricated vapour cell”. In: *Nature Photonics* 1.11 (Nov. 2007), pp. 649–652. ISSN: 17494885. DOI: 10.1038/nphoton.2007.201. URL: <https://www.nature.com/articles/nphoton.2007.201>.
- [97] Rujie Li et al. “Continuous high-sensitivity and high-bandwidth atomic magnetometer”. In: *Physical Review Applied* 14.6 (Dec. 2020), p. 064067. ISSN: 23317019. DOI: <https://doi.org/10.1103/PhysRevApplied.14.064067>. URL: <https://journals.aps.org/prapplied/abstract/10.1103/PhysRevApplied.14.064067>.
- [98] J. Belfi et al. “Cesium coherent population trapping magnetometer for cardiosignal detection in an unshielded environment”. In: *Journal of the Optical Society of America B* 24.9 (Sept. 2007), p. 2357. ISSN: 0740-3224. DOI: 10.1364/josab.24.002357. URL: <https://www.osapublishing.org/josab/abstract.cfm?uri=josab-24-9-2357>.
- [99] Kiyoshi Ishikawa. “High-temperature lithium atomic magnetometry by symmetric hyperfine coherent population trapping resonances”. In: *Journal of the Optical Society of America B* 38.7 (July 2021), p. 2155. ISSN: 0740-3224. DOI: 10.1364/josab.423749. URL: <https://www.osapublishing.org/josab/abstract.cfm?uri=josab-38-7-2155>.
- [100] Hongying Yang et al. “High bandwidth three-axis magnetometer based on optically polarized 85Rb under unshielded environment”. In: *Journal of Physics D: Applied Physics* 53.6 (Dec. 2020), p. 065002. ISSN: 13616463. DOI: 10.1088/1361-6463/ab541a. URL: <https://iopscience.iop.org/article/10.1088/1361-6463/ab541a>.

- [101] H. C. Huang et al. “Three-axis atomic magnetometer based on spin precession modulation”. In: *Applied Physics Letters* 107.18 (Nov. 2015), p. 182403. ISSN: 00036951. DOI: 10.1063/1.4935096. URL: <https://aip.scitation.org/doi/abs/10.1063/1.4935096>.
- [102] Zhichao Ding, Jie Yuan, and Xingwu Long. “Response of a Bell-Bloom magnetometer to a magnetic field of arbitrary direction”. In: *Sensors (Switzerland)* 18.5 (May 2018), p. 1401. ISSN: 14248220. DOI: 10.3390/s18051401. URL: <https://www.mdpi.com/1424-8220/18/5/1401/htm%20https://www.mdpi.com/1424-8220/18/5/1401>.
- [103] S. J. Seltzer and M. V. Romalis. “Unshielded three-axis vector operation of a spin-exchange-relaxation-free atomic magnetometer”. In: *Applied Physics Letters* 85.20 (Nov. 2004), pp. 4804–4806. ISSN: 00036951. DOI: 10.1063/1.1814434. URL: <https://aip.scitation.org/doi/abs/10.1063/1.1814434>.
- [104] Aram Papoyan et al. “Magnetic-field-compensation optical vector magnetometer”. In: *Applied Optics* 55.4 (Feb. 2016), p. 892. ISSN: 0003-6935. DOI: 10.1364/ao.55.000892. URL: <https://opg.optica.org/ao/abstract.cfm?uri=ao-55-4-892>.
- [105] B. Patton et al. “All-optical vector atomic magnetometer”. In: *Physical Review Letters* 113.1 (July 2014), p. 013001. ISSN: 10797114. DOI: 10.1103/PhysRevLett.113.013001. URL: <https://journals.aps.org/prl/abstract/10.1103/PhysRevLett.113.013001>.
- [106] Tadas Pyragius, Hans Marin Florez, and Thomas Fernholz. “Voigt-effect-based three-dimensional vector magnetometer”. In: *Physical Review A* 100.2 (Aug. 2019), p. 023416. ISSN: 24699934. DOI: 10.1103/PhysRevA.100.023416. URL: <https://journals.aps.org/pra/abstract/10.1103/PhysRevA.100.023416>.
- [107] V. I. Yudin et al. “Vector magnetometry based on electromagnetically induced transparency in linearly polarized light”. In: *Physical Review A - Atomic, Molecular, and Optical Physics* 82.3 (Sept. 2010), p. 033807. ISSN: 10502947. DOI: 10.1103/PhysRevA.82.033807. URL: <https://journals.aps.org/pra/abstract/10.1103/PhysRevA.82.033807>.
- [108] Haje Korth et al. “Miniature atomic scalar magnetometer for space based on the rubidium isotope 87Rb”. In: *Journal of Geophysical Research: Space Physics* 121.8 (Aug. 2016), pp. 7870–7880. ISSN: 21699402. DOI: 10.1002/2016JA022389. URL: <https://agupubs.onlinelibrary.wiley.com/doi/10.1002/2016JA022389>.
- [109] G. Oelsner et al. “Integrated optically pumped magnetometer for measurements within Earth’s magnetic field”. In: *Physical Review Applied* 17.2 (Feb. 2022), p. 024034. ISSN: 23317019. DOI: 10.1103/physrevapplied.17.024034. URL: <https://journals.aps.org/prapplied/abstract/10.1103/PhysRevApplied.17.024034>.
- [110] Peter D.D. Schwindt et al. “Chip-scale atomic magnetometer with improved sensitivity by use of the Mx technique”. In: *Applied Physics Letters* 90.8 (Feb. 2007), p. 081102. ISSN: 00036951. DOI: 10.1063/1.2709532. URL: <https://aip.scitation.org/doi/abs/10.1063/1.2709532>.
- [111] Ricardo Jiménez-Martínez et al. “Sensitivity comparison of Mx and frequency-modulated bell-bloom Cs magnetometers in a microfabricated cell”. In: *IEEE Transactions on Instrumentation and Measurement* 59.2 (Feb. 2010), pp. 372–378. ISSN: 00189456. DOI: 10.1109/TIM.2009.2023829. URL: <https://ieeexplore.ieee.org/document/5247087>.

- [112] Vladislav Gerginov, Sean Krzyzewski, and Svenja Knappe. “Pulsed operation of a miniature scalar optically pumped magnetometer”. In: *Journal of the Optical Society of America B* 34.7 (July 2017), p. 1429. ISSN: 0740-3224. DOI: 10.1364/josab.34.001429. URL: <https://www.osapublishing.org/josab/abstract.cfm?uri=josab-34-7-1429>.
- [113] Vladislav Gerginov, Marco Pomponio, and Svenja Knappe. “Scalar magnetometry below 100 fT/sqrt(Hz) in a microfabricated cell”. In: *IEEE Sensors Journal* 20.21 (Nov. 2020), pp. 12684–12690. ISSN: 15581748. DOI: 10.1109/JSEN.2020.3002193. URL: <https://ieeexplore.ieee.org/document/9117011>.
- [114] Jin Zhang et al. “Magnetocardiography measurements by microfabricated atomic magnetometer with a 3-D spherical alkali vapor cell”. In: *IEEE Transactions on Instrumentation and Measurement* 70 (2021). ISSN: 15579662. DOI: 10.1109/TIM.2021.3120375. URL: <https://ieeexplore.ieee.org/document/9585396>.
- [115] Yoel Sebbag et al. “Demonstration of an integrated nanophotonic chip-scale alkali vapor magnetometer using inverse design”. In: *Light: Science and Applications* 10.1 (Mar. 2021), pp. 1–8. ISSN: 20477538. DOI: 10.1038/s41377-021-00499-5. URL: <https://www.nature.com/articles/s41377-021-00499-5>.
- [116] Peter D.D. Schwindt et al. “Chip-scale atomic magnetometer”. In: *Applied Physics Letters* 85.26 (Dec. 2004), pp. 6409–6411. ISSN: 00036951. DOI: 10.1063/1.1839274. URL: <https://aip.scitation.org/doi/abs/10.1063/1.1839274>.
- [117] Hyun Gue Hong et al. “Chip-scale ultra-low field atomic magnetometer based on coherent population trapping”. In: *Sensors* 21.4 (Feb. 2021), pp. 1–10. ISSN: 14248220. DOI: 10.3390/s21041517. URL: <https://www.mdpi.com/1424-8220/21/4/1517>.
- [118] Jean Brossel and Francis Bitter. “A New ”Double Resonance” Method for Investigating Atomic Energy Levels. Application to Hg 3P1”. In: *Physical Review* 86.3 (May 1952), p. 308. ISSN: 0031899X. DOI: 10.1103/PhysRev.86.308. URL: <https://journals.aps.org/pr/abstract/10.1103/PhysRev.86.308>.
- [119] Alan Corney. *Atomic and Laser Spectroscopy*. Oxford University Press, 2006.
- [120] J. H. Allen and P. L. Bender. “Narrow line rubidium magnetometer for high accuracy field measurements”. In: *Journal of geomagnetism and geoelectricity* 24.1 (1972), pp. 105–125. ISSN: 00221392. DOI: 10.5636/jgg.24.105. URL: https://www.jstage.jst.go.jp/article/jgg1949/24/1/24_1_105/_article.
- [121] E. Pulz, K. H. Jäckel, and H. J. Linthe. “A new optically pumped tandem magnetometer: Principles and experiences”. In: *Measurement Science and Technology* 10.11 (Nov. 1999), pp. 1025–1031. ISSN: 09570233. DOI: 10.1088/0957-0233/10/11/309. URL: <https://iopscience.iop.org/article/10.1088/0957-0233/10/11/309>.
- [122] W. Chalupczak et al. “Room temperature femtotesla radio-frequency atomic magnetometer”. In: *Applied Physics Letters* 100.24 (June 2012), p. 242401. ISSN: 00036951. DOI: 10.1063/1.4729016. URL: <https://aip.scitation.org/doi/abs/10.1063/1.4729016>.
- [123] Zoran D. Grujić et al. “A sensitive and accurate atomic magnetometer based on free spin precession”. In: *European Physical Journal D* 69.5 (May 2015), pp. 1–10. ISSN: 14346079. DOI: 10.1140/epjd/e2015-50875-3. URL: <https://link.springer.com/article/10.1140/epjd/e2015-50875-3>.

- [124] J. Belfi et al. “Dual channel self-oscillating optical magnetometer”. In: *Journal of the Optical Society of America B* 26.5 (May 2009), p. 910. ISSN: 0740-3224. DOI: 10.1364/josab.26.000910. URL: <https://www.osapublishing.org/josab/abstract.cfm?uri=josab-26-5-910>.
- [125] Vishal Shah et al. “Fully integrated standalone zero field optically pumped magnetometer for biomagnetism”. In: *Proc. SPIE 10548, Steep Dispersion Engineering and Opto-Atomic Precision Metrology XI* 10548 (Feb. 2018), 105481G. ISSN: 1996756X. DOI: 10.1117/12.2299197. URL: <https://www.spiedigitallibrary.org/conference-proceedings-of-spie/10548/105481G/Fully-integrated-standalone-zero-field-optically-pumped-magnetometer-for-biomagnetism/10.1117/12.2299197.short>.
- [126] Volkmar Schultze et al. “Characteristics and performance of an intensity-modulated optically pumped magnetometer in comparison to the classical Mx magnetometer”. In: *Optics Express* 20.13 (June 2012), p. 14201. ISSN: 1094-4087. DOI: 10.1364/oe.20.014201. URL: <https://opg.optica.org/oe/abstract.cfm?uri=oe-20-13-14201&id=238230>.
- [127] Ricardo Jiménez-Martínez et al. “High-bandwidth optical magnetometer”. In: *Journal of the Optical Society of America B* 29.12 (Dec. 2012), p. 3398. ISSN: 0740-3224. DOI: 10.1364/josab.29.003398. URL: <https://www.osapublishing.org/josab/abstract.cfm?uri=josab-29-12-3398>.
- [128] G. Bison, R. Wynands, and A. Weis. “Dynamical mapping of the human cardiomagnetic field with a room-temperature, laser-optical sensor”. In: *Optics Express* 11.8 (Apr. 2003), p. 904. ISSN: 10944087. DOI: 10.1364/oe.11.000904. URL: <https://www.osapublishing.org/oe/abstract.cfm?uri=oe-11-8-904>.
- [129] Jingwei Sheng et al. “Magnetoencephalography with a Cs-based high-sensitivity compact atomic magnetometer”. In: *Review of Scientific Instruments* 88.9 (Sept. 2017). ISSN: 10897623. DOI: 10.1063/1.5001730. URL: <https://pubmed.ncbi.nlm.nih.gov/28964239>.
- [130] Mikhail V. Petrenko et al. “Towards the non-zero field cesium magnetic sensor array for magnetoencephalography”. In: *IEEE Sensors Journal* 21.17 (Sept. 2021), pp. 18626–18632. ISSN: 15581748. DOI: 10.1109/JSEN.2021.3089455. URL: <https://ieeexplore.ieee.org/document/9455403>.
- [131] Victor Lebedev, Stefan Hartwig, and Thomas Middelmann. “Fast and robust optically pumped cesium magnetometer”. In: *Advanced Optical Technologies* 9.5 (Oct. 2020), pp. 275–286. ISSN: 21928584. DOI: 10.1515/aot-2020-0024. URL: <https://www.degruyter.com/document/doi/10.1515/aot-2020-0024/html>.
- [132] Simone Colombo et al. “Towards a mechanical MPI scanner based on atomic magnetometry”. In: *International Journal on Magnetic Particle Imaging* 3.1 (2016). URL: <https://journal.iwmpi.org/index.php/iwmpi/article/view/77>.
- [133] Michael C.D. Tayler et al. “Invited Review Article: Instrumentation for nuclear magnetic resonance in zero and ultralow magnetic field”. In: *Review of Scientific Instruments* 88.9 (Sept. 2017), p. 091101. ISSN: 10897623. DOI: 10.1063/1.5003347. URL: <https://aip.scitation.org/doi/abs/10.1063/1.5003347>.

- [134] Sven Bodenstedt, Morgan W. Mitchell, and Michael C.D. Tayler. “Fast-field-cycling ultralow-field nuclear magnetic relaxation dispersion”. In: *Nature Communications* 12.1 (June 2021), pp. 1–8. ISSN: 20411723. DOI: 10.1038/s41467-021-24248-9. URL: <https://www.nature.com/articles/s41467-021-24248-9>.
- [135] Ethan J Pratt et al. “Kernel Flux: a whole-head 432-magnetometer optically-pumped magnetoencephalography (OP-MEG) system for brain activity imaging during natural human experiences”. In: *Proc. SPIE 11700, Optical and Quantum Sensing and Precision Metrology*. Vol. 11700. 5. SPIE, Mar. 2021, p. 1170032. ISBN: 9781510642355. DOI: 10.1117/12.2581794. URL: <https://www.spiedigitallibrary.org/conference-proceedings-of-spie/11700/1170032/Kernel-Flux--a-whole-head-432-magnetometer-optically-pumped/10.1117/12.2581794.full>.
- [136] Anna U. Kowalczyk et al. “Detection of human auditory evoked brain signals with a resilient nonlinear optically pumped magnetometer”. In: *NeuroImage* 226 (Feb. 2021), p. 117497. ISSN: 10959572. DOI: 10.1016/j.neuroimage.2020.117497. URL: <https://www.sciencedirect.com/science/article/pii/S1053811920309824>.
- [137] Amir Borna et al. “A 20-channel magnetoencephalography system based on optically pumped magnetometers”. In: *Physics in Medicine and Biology* 62.23 (Nov. 2017), pp. 8909–8923. ISSN: 13616560. DOI: 10.1088/1361-6560/aa93d1. URL: <https://iopscience.iop.org/article/10.1088/1361-6560/aa93d1>.
- [138] Stuart Ingleby et al. “A digital alkali spin maser”. In: *Scientific Reports* 2022 12:1 12.1 (July 2022), pp. 1–7. ISSN: 2045-2322. DOI: 10.1038/s41598-022-16910-z. URL: <https://www.nature.com/articles/s41598-022-16910-z>.
- [139] G. Oelsner et al. “Sources of heading errors in optically pumped magnetometers operated in the Earth’s magnetic field”. In: *Physical Review A* 99.1 (Jan. 2019), p. 013420. ISSN: 24699934. DOI: 10.1103/PhysRevA.99.013420. URL: <https://journals.aps.org/pr/abstract/10.1103/PhysRevA.99.013420>.
- [140] W. Lee et al. “Heading errors in all-optical alkali-metal-vapor magnetometers in geomagnetic fields”. In: *Physical Review A* 103.6 (June 2021), p. 063103. ISSN: 24699934. DOI: 10.1103/PhysRevA.103.063103. URL: <https://journals.aps.org/pr/abstract/10.1103/PhysRevA.103.063103>.
- [141] Guzhi Bao et al. “Suppression of the nonlinear Zeeman effect and heading error in Earth-field-range alkali-vapor magnetometers”. In: *Physical Review Letters* 120.3 (Jan. 2018), p. 033202. ISSN: 10797114. DOI: 10.1103/PhysRevLett.120.033202. URL: <https://journals.aps.org/prl/abstract/10.1103/PhysRevLett.120.033202>.
- [142] Ricardo Jiménez-Martínez et al. “Signal tracking beyond the time resolution of an atomic sensor by Kalman filtering”. In: *Physical Review Letters* 120.4 (Jan. 2018), p. 040503. ISSN: 10797114. DOI: 10.1103/PhysRevLett.120.040503. URL: <https://journals.aps.org/prl/abstract/10.1103/PhysRevLett.120.040503>.
- [143] Cameron Deans, Luca Marmugi, and Ferruccio Renzoni. “Active underwater detection with an array of atomic magnetometers”. In: *Applied Optics* 57.10 (Apr. 2018), p. 2346. ISSN: 1559-128X. DOI: 10.1364/ao.57.002346. URL: <https://opg.optica.org/ao/abstract.cfm?uri=ao-57-10-2346>.
- [144] Armen Sargsyan et al. “Selective reflection from an Rb layer with a thickness below $\lambda/12$ and applications”. In: *Optics Letters* 42.8 (Apr. 2017), p. 1476. ISSN: 0146-9592. DOI: 10.1364/ol.42.001476. URL: <https://opg.optica.org/ol/abstract.cfm?uri=ol-42-8-1476>.

- [145] Seth DeVore et al. “Improving student understanding of lock-in amplifiers”. In: *American Journal of Physics* 84.1 (Dec. 2016), pp. 52–56. ISSN: 0002-9505. DOI: 10.1119/1.4934957. URL: <https://aapt.scitation.org/doi/abs/10.1119/1.4934957>.
- [146] Wenhao Li et al. “Characterization of high-temperature performance of cesium vapor cells with anti-relaxation coating”. In: *Journal of Applied Physics* 121.6 (Feb. 2017), p. 063104. ISSN: 10897550. DOI: 10.1063/1.4976017. URL: <https://aip.scitation.org/doi/abs/10.1063/1.4976017>.
- [147] A. B. Matsko et al. “Radiation Trapping in Coherent Media”. In: *Physical Review Letters* 87.13 (Sept. 2001), p. 133601. ISSN: 0031-9007. DOI: 10.1103/PhysRevLett.87.133601.
- [148] Runqi Han et al. “Is light narrowing possible with dense-vapor paraffin coated cells for atomic magnetometers?” In: *AIP Advances* 7.12 (Dec. 2017), p. 125224. ISSN: 21583226. DOI: 10.1063/1.4997691. URL: <https://aip.scitation.org/doi/abs/10.1063/1.4997691>.
- [149] M. P. Ledbetter et al. “Zero-field remote detection of NMR with a microfabricated atomic magnetometer”. In: *Proceedings of the National Academy of Sciences of the United States of America* 105.7 (Feb. 2008), pp. 2286–2290. ISSN: 00278424. DOI: 10.1073/pnas.0711505105. URL: <https://www.pnas.org/content/105/7/2286%20https://www.pnas.org/content/105/7/2286.abstract>.
- [150] D. V. Brazhnikov et al. “Level-crossing resonances on open atomic transitions in a buffered Cs vapor cell: Linewidth narrowing, high contrast, and atomic magnetometry applications”. In: *Physical Review A* 106.1 (July 2022), p. 013113. ISSN: 24699934. DOI: 10.1103/PhysRevA.106.013113. URL: <https://journals.aps.org/pra/abstract/10.1103/PhysRevA.106.013113>.
- [151] Kaleb Campbell et al. “Intrinsic pulsed magnetic gradiometer in Earth’s field”. In: *arXiv* (Nov. 2021). DOI: 10.48550/arxiv.2111.12310. URL: <https://arxiv.org/abs/2111.12310v1>.
- [152] S. Woetzel et al. “Microfabricated atomic vapor cell arrays for magnetic field measurements”. In: *Review of Scientific Instruments* 82.3 (Mar. 2011), p. 033111. ISSN: 00346748. DOI: 10.1063/1.3559304. URL: <https://aip.scitation.org/doi/abs/10.1063/1.3559304>.
- [153] Sylvain Karlen et al. “Lifetime assessment of RbN₃-filled MEMS atomic vapor cells with Al₂O₃ coating”. In: *Optics Express* 25.3 (Feb. 2017), p. 2187. ISSN: 10944087. DOI: 10.1364/oe.25.002187. URL: <https://opg.optica.org/oe/abstract.cfm?uri=oe-25-3-2187>.
- [154] R. Vicarini et al. “Demonstration of the mass-producible feature of a Cs vapor microcell technology for miniature atomic clocks”. In: *Sensors and Actuators, A: Physical* 280 (Sept. 2018), pp. 99–106. ISSN: 09244247. DOI: 10.1016/j.sna.2018.07.032. URL: <https://www.sciencedirect.com/science/article/abs/pii/S0924424718305387>.
- [155] Kasper Jensen et al. “Non-invasive detection of animal nerve impulses with an atomic magnetometer operating near quantum limited sensitivity”. In: *Scientific Reports* 6.1 (July 2016), pp. 1–7. ISSN: 20452322. DOI: 10.1038/srep29638. URL: <https://www.nature.com/articles/srep29638>.

- [156] Eric D. Black. “An introduction to Pound–Drever–Hall laser frequency stabilization”. In: *American Journal of Physics* 69.1 (Dec. 2001), pp. 79–87. ISSN: 0002-9505. DOI: 10.1119/1.1286663. URL: <https://aapt.scitation.org/doi/abs/10.1119/1.1286663>.
- [157] Silvia Knappe-Grueneberg et al. “Influence of demagnetization coil configuration on residual field in an extremely magnetically shielded room: Model and measurements”. In: *Journal of Applied Physics* 103.7 (Mar. 2008), 07E925. ISSN: 0021-8979. DOI: 10.1063/1.2837876. URL: <https://aip.scitation.org/doi/abs/10.1063/1.2837876>.
- [158] Niall Holmes et al. “Naturalistic hyperscanning with wearable magnetoencephalography”. In: *bioRxiv* (Sept. 2021), p. 2021.09.07.459124. DOI: 10.1101/2021.09.07.459124. URL: <https://www.biorxiv.org/content/10.1101/2021.09.07.459124v1>.
- [159] L M Rushton et al. “Unshielded portable optically pumped magnetometer for the remote detection of conductive objects using eddy current measurements”. In: *arXiv* (June 2022). DOI: 10.48550/arxiv.2206.04631. URL: <https://arxiv.org/abs/2206.04631v1>.
- [160] Daryl W. Preston. “Doppler-free saturated absorption: Laser spectroscopy”. In: *American Journal of Physics* 64.11 (July 1998), p. 1432. ISSN: 0002-9505. DOI: 10.1119/1.18457. URL: <https://aapt.scitation.org/doi/abs/10.1119/1.18457>.
- [161] Hanna Krauter. “Generation and application of entanglement of room temperature ensembles of atoms”. PhD thesis. Copenhagen: University of Copenhagen, Feb. 2011. URL: https://nbi.ku.dk/english/theses/phd-theses/hanna-krauter/hannah_thesis.pdf.
- [162] Irina Novikova, Andrey B. Matsko, and George R. Welch. “Influence of a buffer gas on nonlinear magneto-optical polarization rotation”. In: *Journal of the Optical Society of America B* 22.1 (Jan. 2005), p. 44. ISSN: 0740-3224. DOI: 10.1364/josab.22.000044. URL: <https://opg.optica.org/josab/abstract.cfm?uri=josab-22-1-44>.
- [163] *GEM GSMP Potassium Magnetometer for High Precision and Accuracy - GEM Systems*. URL: <https://www.gemsys.ca/ultra-high-sensitivity-potassium>.
- [164] M. T. Graf et al. “Relaxation of atomic polarization in paraffin-coated cesium vapor cells”. In: *Physical Review A - Atomic, Molecular, and Optical Physics* 72.2 (Aug. 2005), p. 023401. ISSN: 10502947. DOI: 10.1103/PhysRevA.72.023401. URL: <https://journals.aps.org/pr/abstract/10.1103/PhysRevA.72.023401>.
- [165] M. V. Balabas et al. “Polarized alkali-metal vapor with minute-long transverse spin-relaxation time”. In: *Physical Review Letters* 105.7 (Aug. 2010), p. 070801. ISSN: 00319007. DOI: 10.1103/PhysRevLett.105.070801. URL: <https://journals.aps.org/prl/abstract/10.1103/PhysRevLett.105.070801>.
- [166] S. J. Seltzer et al. “Investigation of antirelaxation coatings for alkali-metal vapor cells using surface science techniques”. In: *Journal of Chemical Physics* 133.14 (Oct. 2010), p. 144703. ISSN: 00219606. DOI: 10.1063/1.3489922. URL: <https://aip.scitation.org/doi/abs/10.1063/1.3489922>.
- [167] N. Castagna et al. “A large sample study of spin relaxation and magnetometric sensitivity of paraffin-coated Cs vapor cells”. In: *Applied Physics B: Lasers and Optics* 96.4 (Apr. 2009), pp. 763–772. ISSN: 09462171. DOI: 10.1007/s00340-009-3464-5. URL: <https://link.springer.com/article/10.1007/s00340-009-3464-5>.

- [168] Dmitry Budker, Donald J. Orlando, and Valeriy Yashchuk. “Nonlinear laser spectroscopy and magneto-optics”. In: *American Journal of Physics* 67.7 (July 1999), pp. 584–592. ISSN: 0002-9505. DOI: 10.1119/1.19328. URL: <https://aapt.scitation.org/doi/abs/10.1119/1.19328>.
- [169] S. Groeger et al. “A sound card based multi-channel frequency measurement system”. In: *The European Physical Journal - Applied Physics* 33.3 (Mar. 2006), pp. 221–224. ISSN: 1286-0042. DOI: 10.1051/EPJAP:2006020. URL: <https://www.cambridge.org/core/journals/the-european-physical-journal-applied-physics/article/abs/sound-card-based-multichannel-frequency-measurement-system/3D3452C22E03D5CCEDF25CB6CA87EC3D>.
- [170] G. Bison et al. “Sensitive and stable vector magnetometer for operation in zero and finite fields”. In: *Optics Express* 26.13 (June 2018), p. 17350. ISSN: 10944087. DOI: 10.1364/oe.26.017350. URL: <https://opg.optica.org/oe/abstract.cfm?uri=oe-26-13-17350>.
- [171] Philip J. Broser et al. “Optically pumped magnetometers for magneto-myography to study the innervation of the hand”. In: *IEEE Transactions on Neural Systems and Rehabilitation Engineering* 26.11 (Nov. 2018), pp. 2226–2230. ISSN: 15344320. DOI: 10.1109/TNSRE.2018.2871947.
- [172] H. Xia et al. “Magnetoencephalography with an atomic magnetometer”. In: *Applied Physics Letters* 89.21 (Nov. 2006), p. 211104. ISSN: 00036951. DOI: 10.1063/1.2392722. URL: <https://aip.scitation.org/doi/abs/10.1063/1.2392722>.
- [173] Elena Boto et al. “Moving magnetoencephalography towards real-world applications with a wearable system”. In: *Nature* 555.7698 (Mar. 2018), pp. 657–661. ISSN: 14764687. DOI: 10.1038/nature26147. URL: <https://www.nature.com/articles/nature26147>.
- [174] M. E. Limes et al. “Portable magnetometry for detection of biomagnetism in ambient environments”. In: *Physical Review Applied* 14.1 (July 2020), p. 011002. ISSN: 23317019. DOI: 10.1103/PhysRevApplied.14.011002. URL: <https://journals.aps.org/prapplied/abstract/10.1103/PhysRevApplied.14.011002>.
- [175] Amir Borna et al. “Non-invasive functional-brain-imaging with an OPM-based magnetoencephalography system”. In: *PLOS ONE* 15.1 (Jan. 2020), e0227684. ISSN: 1932-6203. DOI: 10.1371/JOURNAL.PONE.0227684. URL: <https://journals.plos.org/plosone/article?id=10.1371/journal.pone.0227684>.
- [176] Aikaterini Gialopsou et al. “Improved spatio-temporal measurements of visually evoked fields using optically-pumped magnetometers”. In: *Scientific Reports* 2021 11:1 11.1 (Nov. 2021), pp. 1–11. ISSN: 2045-2322. DOI: 10.1038/s41598-021-01854-7. URL: <https://www.nature.com/articles/s41598-021-01854-7>.
- [177] I. A. Sulai et al. “Characterizing atomic magnetic gradiometers for fetal magnetocardiography”. In: *Review of Scientific Instruments* 90.8 (Aug. 2019), p. 085003. ISSN: 10897623. DOI: 10.1063/1.5091007. URL: <https://aip.scitation.org/doi/abs/10.1063/1.5091007>.
- [178] G Lembke et al. “Optical multichannel room temperature magnetic field imaging system for clinical application”. In: *Biomedical Optics Express* 5.3 (Mar. 2014), p. 876. ISSN: 2156-7085. DOI: 10.1364/boe.5.000876. URL: <https://opg.optica.org/boe/abstract.cfm?uri=boe-5-3-876>.

- [179] Cort Johnson et al. “Magnetic relaxometry with an atomic magnetometer and SQUID sensors on targeted cancer cells”. In: *Journal of Magnetism and Magnetic Materials* 324.17 (Aug. 2012), pp. 2613–2619. ISSN: 03048853. DOI: 10.1016/j.jmmm.2012.03.015. URL: <https://www.sciencedirect.com/science/article/pii/S0304885312002582>.
- [180] Lykourgos Bougas et al. “Nondestructive in-line sub-picomolar detection of magnetic nanoparticles in flowing complex fluids”. In: *Scientific Reports* 8.1 (Feb. 2018), pp. 1–8. ISSN: 20452322. DOI: 10.1038/s41598-018-21802-2. URL: <https://www.nature.com/articles/s41598-018-21802-2>.
- [181] Xin Bi et al. “Quantitative analysis of magnetic cobalt particles with an optically pumped atomic magnetometer”. In: *Applied Physics Letters* 118.8 (Feb. 2021), p. 084101. ISSN: 00036951. DOI: 10.1063/5.0039565. URL: <https://aip.scitation.org/doi/abs/10.1063/5.0039565>.
- [182] Aaron Jaufenthaler et al. “Pulsed optically pumped magnetometers: Addressing dead time and bandwidth for the unshielded magnetorelaxometry of magnetic nanoparticles”. In: *Sensors (Switzerland)* 21.4 (Feb. 2021), pp. 1–19. ISSN: 14248220. DOI: 10.3390/s21041212. URL: <https://www.mdpi.com/1424-8220/21/4/1212/htm%20https://www.mdpi.com/1424-8220/21/4/1212>.
- [183] Eric Corsini et al. “Search for plant biomagnetism with a sensitive atomic magnetometer”. In: *Journal of Applied Physics*. Vol. 109. 7. American Institute of PhysicsAIP, Apr. 2011, p. 074701. DOI: 10.1063/1.3560920. URL: <https://aip.scitation.org/doi/abs/10.1063/1.3560920>.
- [184] Anne Fabricant et al. “Action potentials induce biomagnetic fields in carnivorous Venus flytrap plants”. In: *Scientific Reports* 11.1 (Jan. 2021), pp. 1–7. ISSN: 20452322. DOI: 10.1038/s41598-021-81114-w. URL: <https://www.nature.com/articles/s41598-021-81114-w>.
- [185] Jens U. Sutter et al. “Recording the heart beat of cattle using a gradiometer system of optically pumped magnetometers”. In: *Computers and Electronics in Agriculture* 177 (Oct. 2020), p. 105651. ISSN: 0168-1699. DOI: 10.1016/J.COMPAG.2020.105651. URL: <https://www.sciencedirect.com/science/article/pii/S0168169920311480>.
- [186] John W. Blanchard, Dmitry Budker, and Andreas Trabesinger. “Lower than low: Perspectives on zero- to ultralow-field nuclear magnetic resonance”. In: *Journal of Magnetic Resonance* 323 (Feb. 2021), p. 106886. ISSN: 10907807. DOI: 10.1016/j.jmr.2020.106886. URL: <https://www.sciencedirect.com/science/article/abs/pii/S1090780720302044>.
- [187] I. M. Savukov and M. V. Romalis. “NMR detection with an atomic magnetometer”. In: *Physical Review Letters* 94.12 (Apr. 2005), p. 123001. ISSN: 00319007. DOI: 10.1103/PhysRevLett.94.123001. URL: <https://journals.aps.org/prl/abstract/10.1103/PhysRevLett.94.123001>.
- [188] Shoujun Xu et al. “Magnetic resonance imaging with an optical atomic magnetometer”. In: *Proceedings of the National Academy of Sciences of the United States of America* 103.34 (Aug. 2006), pp. 12668–12671. ISSN: 00278424. DOI: 10.1073/pnas.0605396103. URL: <https://www.pnas.org/content/103/34/12668%20https://www.pnas.org/content/103/34/12668.abstract>.

- [189] Min Jiang et al. “Magnetic gradiometer for the detection of zero- to ultralow-field nuclear magnetic resonance”. In: *Physical Review Applied* 11.2 (Feb. 2019), p. 024005. ISSN: 23317019. DOI: 10.1103/PhysRevApplied.11.024005. URL: <https://journals.aps.org/prapplied/abstract/10.1103/PhysRevApplied.11.024005>.
- [190] S. Begus et al. “Optical detection of low frequency NQR signals: A step forward from conventional NQR”. In: *Journal of Physics D: Applied Physics* 50.9 (Feb. 2017), p. 095601. ISSN: 13616463. DOI: 10.1088/1361-6463/aa4f23. URL: <https://iopscience.iop.org/article/10.1088/1361-6463/aa4f23>.
- [191] Giuseppe Bevilacqua et al. “Sub-millimetric ultra-low-field MRI detected in situ by a dressed atomic magnetometer”. In: *Applied Physics Letters* 115.17 (Oct. 2019), p. 174102. ISSN: 00036951. DOI: 10.1063/1.5123653. URL: <https://aip.scitation.org/doi/abs/10.1063/1.5123653>.
- [192] Danila A. Barskiy et al. “Zero-field nuclear magnetic resonance of chemically exchanging systems”. In: *Nature Communications* 10.1 (July 2019), p. 3002. ISSN: 2041-1723. DOI: 10.1038/s41467-019-10787-9. URL: <https://www.nature.com/articles/s41467-019-10787-9>.
- [193] Piotr Put et al. “Zero- to Ultralow-Field NMR Spectroscopy of Small Biomolecules”. In: *Analytical Chemistry* 93.6 (Feb. 2021), pp. 3226–3232. ISSN: 0003-2700. DOI: 10.1021/acs.analchem.0c04738. URL: <https://pubs.acs.org/doi/10.1021/acs.analchem.0c04738>.
- [194] Rui Zhang et al. “Stand-off magnetometry with directional emission from sodium vapors”. In: *Physical Review Letters* 127.17 (Oct. 2021), p. 173605. ISSN: 10797114. DOI: 10.1103/PhysRevLett.127.173605. URL: <https://journals.aps.org/prl/abstract/10.1103/PhysRevLett.127.173605>.
- [195] James S. Bennett et al. “Precision magnetometers for aerospace applications: A review”. In: *Sensors* 21.16 (Aug. 2021), p. 5568. ISSN: 14248220. DOI: 10.3390/s21165568. URL: <https://www.mdpi.com/1424-8220/21/16/5568/htm%20https://www.mdpi.com/1424-8220/21/16/5568>.
- [196] Felipe Pedreros Bustos et al. “Polarization-driven spin precession of mesospheric sodium atoms”. In: *Optics Letters* 43.23 (Dec. 2018), p. 5825. ISSN: 0146-9592. DOI: 10.1364/ol.43.005825. URL: <https://opg.optica.org/ol/abstract.cfm?uri=ol-43-23-5825>.
- [197] Luca Marmugi and Ferruccio Renzoni. “Electromagnetic induction imaging with atomic magnetometers: Progress and perspectives”. In: *Applied Sciences (Switzerland)* 10.18 (Sept. 2020), p. 6370. ISSN: 20763417. DOI: 10.3390/APP10186370. URL: <https://www.mdpi.com/2076-3417/10/18/6370/htm%20https://www.mdpi.com/2076-3417/10/18/6370>.
- [198] Kasper Jensen et al. “Detection of low-conductivity objects using eddy current measurements with an optical magnetometer”. In: *Physical Review Research* 1.3 (Nov. 2019), p. 033087. ISSN: 26431564. DOI: 10.1103/PhysRevResearch.1.033087. URL: <https://journals.aps.org/prresearch/abstract/10.1103/PhysRevResearch.1.033087>.
- [199] Giuseppe Bevilacqua et al. “Electromagnetic induction imaging: signal detection based on tuned-dressed optical magnetometry”. In: *Optics Express, Vol. 29, Issue 23, pp. 37081-37090* 29.23 (Nov. 2021), pp. 37081–37090. ISSN: 1094-4087. DOI: 10.1364/OE.437930. URL: <https://opg.optica.org/oe/abstract.cfm?uri=oe-29-23-37081>.

- [200] Benjamin Maddox, Yuval Cohen, and Ferruccio Renzoni. “Through-skin pilot-hole detection and localization with a mechanically translatable atomic magnetometer”. In: *Applied Physics Letters* 120.1 (Jan. 2022), p. 014002. ISSN: 0003-6951. DOI: 10.1063/5.0081274. URL: <https://aip.scitation.org/doi/abs/10.1063/5.0081274>.
- [201] S. Afach et al. “Characterization of the global network of optical magnetometers to search for exotic physics (GNOME)”. In: *Physics of the Dark Universe* 22 (Dec. 2018), pp. 162–180. ISSN: 22126864. DOI: 10.1016/j.dark.2018.10.002. URL: <https://www.sciencedirect.com/science/article/pii/S2212686418301031>.
- [202] Derek F. Jackson Kimball et al. “Constraints on long-range spin-gravity and monopole-dipole couplings of the proton”. In: *Physical Review D* 96.7 (Oct. 2017), p. 075004. ISSN: 24700029. DOI: 10.1103/PhysRevD.96.075004. URL: <https://journals.aps.org/prd/abstract/10.1103/PhysRevD.96.075004>.
- [203] Wolfgang Klassen. *All-Optical Cs Magnetometry System for a Neutron Electric Dipole Moment Experiment - Master thesis, University of Manitoba*. Winnipeg, Canada, Mar. 2020. URL: <https://mspace.lib.umanitoba.ca/handle/1993/34596>.
- [204] Samer Afach et al. “Search for topological defect dark matter with a global network of optical magnetometers”. In: *Nature Physics* 17.12 (Dec. 2021), pp. 1396–1401. ISSN: 17452481. DOI: 10.1038/s41567-021-01393-y. URL: <https://www.nature.com/articles/s41567-021-01393-y>.
- [205] A. Kuzmich et al. “Quantum nondemolition measurements of collective atomic spin”. In: *Physical Review A - Atomic, Molecular, and Optical Physics* 60.3 (Sept. 1999), pp. 2346–2350. ISSN: 10941622. DOI: 10.1103/PhysRevA.60.2346. URL: <https://journals.aps.org/prd/abstract/10.1103/PhysRevA.60.2346>.
- [206] Paul Siddons et al. “A gigahertz-bandwidth atomic probe based on the slow-light Faraday effect”. In: *Nature Photonics* 3.4 (Mar. 2009), pp. 225–229. ISSN: 17494885. DOI: 10.1038/nphoton.2009.27. URL: <https://www.nature.com/articles/nphoton.2009.27>.
- [207] Ming-Feng Wang, Nian-Quan Jiang, and Yi-Zhuang Zheng. “Optical continuous-variable quadratic phase gate via Faraday interaction”. In: *Optics Express* 22.8 (Apr. 2014), p. 9182. ISSN: 10944087. DOI: 10.1364/oe.22.009182. URL: <https://opg.optica.org/oe/abstract.cfm?uri=oe-22-8-9182>.
- [208] Anne Fabricant. *Quantum-Limited Optical Magnetometry with Cesium Microcells - Master thesis, Center for Quantop Optics (QUANTOP), Niels Bohr Institute*. Copenhagen, Denmark, 2014.

Appendix A. Optical pumping in cesium

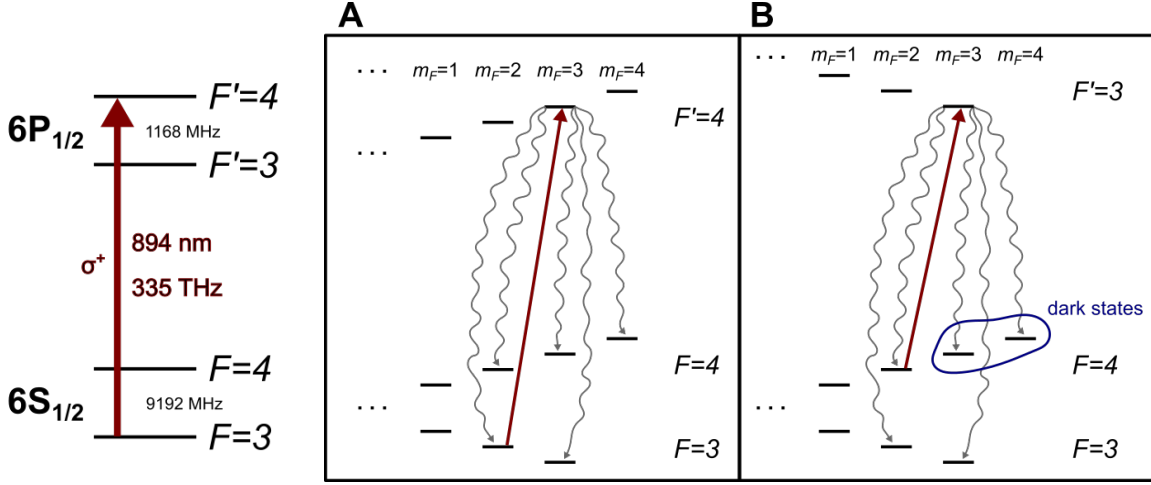


Figure A1: Example of optical pumping on the cesium D1 line (see Sec. 2 for notation and further details), illustrating one of the excitations and associated decay paths. Here we do not consider the possible presence of buffer gas, which may complicate the pumping process in an atomic vapor cell. A) Right-circularly polarized light tuned to the $F = 3 \rightarrow F' = 4$ transition tends to pump the atom into the extreme hyperfine substate $F = 3, m_F = 3$. This particular transition is “leaky” because an excited atom may also decay to the $F = 4$ ground state. B) Pumping on the $F = 4 \rightarrow F' = 3$ transition is preferred since it allows us to make use of the “dark states” $F = 4, m_F = 3$ and $m_F = 4$.

Appendix B. Sensitivity of an atomic magnetometer

How does the sensitivity of the magnetometer scale with the number of atoms N and the measurement time τ ?

Here we choose \hat{x} as atomic-spin polarization (pump) axis, \hat{y} as magnetic-field direction, and \hat{z} as probe direction, as shown in Fig. B1. This is a typical geometry for SERF magnetometers (Table 2), although the same derivation is possible for other operating modes.

After polarizing an atom along \hat{x} , we want to measure the angular-momentum projection $m_F = F, F - 1, \dots, -F$ along \hat{z} for some measurement duration τ . Meanwhile, the atomic spin is evolving under the influence of the external magnetic field \vec{B} according to the Bloch equation (Sec. 2.2):

$$\frac{d\vec{F}}{dt} = \gamma \vec{B} \times \vec{F}. \quad (\text{B.1})$$

The gyromagnetic ratio γ of the atomic system can also be expressed as $\gamma = g \mu_B / \hbar$, where g is the ground-state Landé factor and μ_B is the Bohr magneton. For simplicity, we initially assume a static magnetic field.

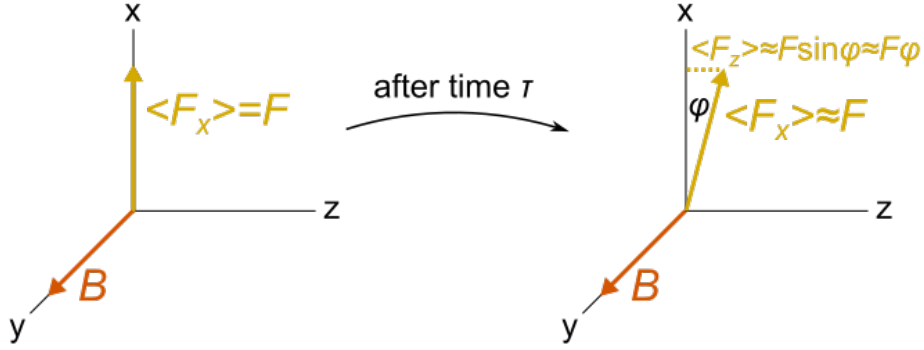


Figure B1: Spin evolution in an atomic magnetometer.

Treating the expectation value of the angular momentum as a classical vector, we find for the evolution of $\langle F_z \rangle$:

$$\frac{d\langle F_z \rangle}{dt} = -\gamma B \langle F_x \rangle. \quad (\text{B.2})$$

Starting from $\langle F_z \rangle = 0$ because the atom is polarized along \hat{x} , and integrating over a small measurement time τ during which $\langle F_x \rangle$ can be considered constant (practically speaking, a time much less than the longitudinal spin-relaxation time T_1), we obtain

$$\langle F_z(\tau) \rangle = -\gamma B \langle F_x \rangle \tau. \quad (\text{B.3})$$

Looking at Fig. B1, which shows the spin precession angle ϕ , we see that

$$\sin \phi \approx \langle F_z \rangle / \langle F_x \rangle \approx \phi. \quad (\text{B.4})$$

Setting $F \approx \langle F_x \rangle \sim 1$ for an order-of-magnitude (for our example of cesium, we typically have $F = 4$), we end up with the following expression:

$$\phi \approx \gamma B \tau. \quad (\text{B.5})$$

This spin precession may be detected via optical rotation or some other technique; in any case we assume that our magnetometer has 100% detection efficiency. (Note that for polarization-based detection, the angle of optical rotation of the probe light is proportional to ϕ .) Hence the uncertainty in B depends on the uncertainty in ϕ :

$$\delta B \approx \frac{\delta \phi}{\gamma \tau}. \quad (\text{B.6})$$

The same result can also be derived for a magnetic field $\vec{B} = B \cos(\Omega t) \hat{y}$ oscillating at the Larmor frequency Ω . Then we find

$$\frac{d\langle F_z \rangle}{dt} = -\gamma B \langle F_x \rangle \frac{\sin(\Omega \tau)}{\Omega}. \quad (\text{B.7})$$

Taking $F \sim 1$ as before and noting that typically $\Omega t \ll 1$, we arrive again at Eq. B.5.

If we are limited only by the quantum noise of the atom (spin-projection noise, Sec. 3.1), $\delta\phi$ is fundamentally set by the Heisenberg uncertainty relation:

$$\Delta F_y \Delta F_z \geq \frac{\langle F_x \rangle}{2}, \quad (\text{B.8})$$

or, assuming minimum uncertainty $\Delta F_y = \Delta F_z$,

$$\Delta F_z = \sqrt{\frac{\langle F_x \rangle}{2}} \approx \sqrt{\frac{F}{2}} \sim 1. \quad (\text{B.9})$$

We also have

$$\Delta F_z \approx F \delta\phi \sim \delta\phi, \quad (\text{B.10})$$

such that we find an uncertainty (standard deviation) in the precession angle of order 1 rad, i.e. $\delta\phi \sim 1$. So Eq. B.6 becomes

$$\delta B \approx \frac{1}{\gamma \tau}. \quad (\text{B.11})$$

Basic statistics tells us that if we perform the same measurement on N independent atoms, the total measurement uncertainty (standard error) improves by \sqrt{N} . Similarly, if we repeatedly perform measurements of duration τ for a total time t , we gain another factor of $\sqrt{t/\tau}$. Thus we arrive at the total sensitivity

$$\delta B_{\text{PN}} = \delta B \frac{1}{\sqrt{N}} \frac{1}{\sqrt{t/\tau}} \approx \frac{1}{\gamma} \frac{1}{\sqrt{N} \tau t} = \frac{\hbar}{g \mu_B} \frac{1}{\sqrt{N} \tau t}. \quad (\text{B.12})$$

Although we would like τ to be as long as possible, in reality this time is limited by the coherence time T_2 of the atomic ensemble, and therefore

$$\delta B_{\text{PN}} \approx \frac{\hbar}{g \mu_B} \frac{1}{\sqrt{N} T_2 t}. \quad (\text{B.13})$$

Appendix C. Data-analysis example

See the provided data file “MagData.bin” and accompanying Mathematica analysis notebook “MagAnalysis.nb”, used to produce the results in Sec. 6.